

**COMPUTATIONAL FLUID DYNAMICS MODELING
OF THERMO-CHEMICAL PROCESSES IN AN
UPDRAFT BIOMASS GASIFIER**

Niranjan Fernando



148009L
University of Moratuwa, Sri Lanka.
Electronic Theses & Dissertations
www.lib.mrt.ac.lk

Thesis submitted in partial fulfillment of the requirements for the Degree Master of
Science

Department of Chemical and Process Engineering

University of Moratuwa

Sri Lanka

November 2015

DECLARATION OF THE CANDIDATE AND SUPERVISOR

I declare that this is my own work and this thesis does not incorporate without acknowledgement any material previously submitted for a Degree or Diploma in any other University or institute of higher learning and to the best of my knowledge and belief it does not contain any material previously published or written by another person except where the acknowledgement is made in the text.

Also, I hereby grant to University of Moratuwa the non-exclusive right to reproduce and distribute my thesis, in whole or in part in print, electronic or other medium. I retain the right to use this content in whole or part in future works (such as articles or books).

Signature:

Date:

The above candidate has carried out research for the Masters thesis under my supervision.



University of Moratuwa, Sri Lanka.
Electronic Theses & Dissertations
www.lib.mrt.ac.lk

Signature of the supervisor:

Date

ABSTRACT

Biomass is recently gaining popularity in industry as a promising source of renewable energy. Gasification of biomass is a major thermal conversion method to improve the efficiency of raw biomass fuel. It is a process by which biomass is partially oxidized to produce a combustible gas named Syngas; a mixture of carbon monoxide, hydrogen and methane. Although the gasification technology is used throughout the history and there are a large number of gasification plants worldwide, their smooth operation remains questionable. This is due to a lack of understanding of proper design criteria. In order to gain insights to optimal design parameters, mathematical models and computer simulations based performance analysis can be used. Recently Computational Fluid Dynamics (CFD) analysis has been applied by many researchers as a tool for optimizing packed bed processes including gasification process. In this research study, a two dimensional CFD model has been developed for an updraft biomass gasifier. The model uses air as the gasifying medium and a fixed batch of biomass. The model is capable of tracking the movement of interface between solid packed bed and gas free board due to bed shrinkage. The two phase model is developed using the Euler-Euler approach. The model consists of several sub models, including reaction models, turbulence model for packed bed gas phase and free board, a radiation model for solid phase, a bed shrinkage model, and interphase heat transfer models. The final mathematical model is converted into a numerical model using open source CFD tool OpenFOAM. Required code was developed by using C++ language in OpenFOAM package, including all the relevant differential equations and procedures in the CFD model. To validate the CFD model, simulation results for gas temperature and gas compositions are compared against experimental gas temperatures and compositions measured from an operational laboratory gasifier. The validated model is used to perform air flow rate optimization. A series of CFD simulations were performed for air flow rates ranging from 3 m³/hr to 10 m³/hr for a computational geometry corresponding to the experimental gasifier and cumulative CO was calculated. It is found that cumulative CO production maximized at 7 m³/hr airflow rate. The maximum cumulative CO volume was 6.4 m³.

Keywords: Biomass, Gasification, Mathematical Model, Computational Fluid Dynamics

DEDICATION

This thesis is dedicated to my beloved mother and to the loving memory of my father



University of Moratuwa, Sri Lanka.
Electronic Theses & Dissertations
www.lib.mrt.ac.lk

ACKNOWLEDGEMENT

I would like to take this opportunity to thank those who have offered me immense support during my research work. First of all, I offer my sincere thanks to my supervisor, Dr. MahinsasaNarayana, Senior lecturer, Department of Chemical and Process Engineering, University of Moratuwa, for his immense guidance and support throughout my research work. I would like to thank Dr. P. G. Rathnasiri, Head, Department of Chemical and Process Engineering, University of Moratuwa for his kind cooperation. I am grateful to Dr. ChathuraRanasinghewho was a member of my progress review committee for his valuable suggestions and advice given to me during my progress reviews. I also thank Dr. ManishaGunasekera, Coordinator of post graduate studies, Senior Lecturer, Department of Chemical and Process Engineering for her corporation. I am grateful to Dr. SanathJayasena, for his valuable support in setting up the high performance computing facility.

I offer my thanks to Mr. Muhammad Amin, for sharing the experimental data from his work and Ms. ThamaliRajika, for her support and advice during my research work.



University of Moratuwa, Sri Lanka.
Electronic Theses & Dissertations

www.lib.mrt.ac.lk

I am grateful to Mr.ChinthakaNarangoda, System Analyst, Department of Chemical and Process Engineering, University of Moratuwa and the staff of Process Control Laboratory of Chemical Engineering Department for their valuable support.

Finally, I am grateful to my mother and brother for their valuable support and encouragement.

Niranjan Fernando

TABLE OF CONTENTS

| | |
|---|------|
| Declaration of the candidate and supervisor | i |
| Abstract | ii |
| Dedication | iii |
| Acknowledgement | iv |
| Table of contents | v |
| List of Figures | viii |
| List of Tables | x |
| Nomenclature | xi |
| List of Appendices | xii |
| 1. Introduction | 1 |
| 1.1 Use of biomass as a renewable energy source | 1 |
| 1.2 Biomass gasification | 2 |
| 1.3 Gasifier types | 3 |
| 1.3.1 Fixed bed gasifiers | 4 |
| 1.3.1.1 Updraft gasifiers | 4 |
| 1.3.1.2 Downdraft gasifiers | 5 |
| 1.3.1.3 Cross flow gasifiers | |
| 1.3.2 Parameters affecting the quality of the produced gas | 6 |
| 1.4 Computational fluid dynamics modeling as a tool to optimize gasifiers | 7 |
| 1.5 Objectives of research | 9 |
| 1.6 A summary of the presented research | 9 |
| 2. Review of packed bed models | 11 |
| 2.1 Modeling approaches | 11 |
| 2.2 Governing transport equations | 13 |
| 2.2.1 Momentum conservation equation | 13 |
| 2.2.2 Temperature equation | 16 |
| 2.2.3 Species conservation equations | 19 |
| 2.3 Reaction rate models | 21 |

| | | |
|-------|--|----|
| 2.4 | Drying | 22 |
| 2.4.1 | First order kinetic model | 22 |
| 2.4.2 | Equilibrium model | 22 |
| 2.5 | Pyrolysis | 23 |
| 2.6 | Heterogeneous reactions: Combustion and Gasification | 26 |
| 2.7 | Homogenous reactions | 27 |
| 3. | Mathematical model for the packed bed | 29 |
| 3.1 | Computational domain and model description | 29 |
| 3.2 | Governing transport equations | 30 |
| 3.3 | Drying model | 31 |
| 3.3.1 | Assumptions used for calculating k_m | 33 |
| 3.3.2 | Assumptions used for calculating x^* | 34 |
| 3.4 | Pyrolysis model | 35 |
| 3.5 | Interphase heat transfer | 35 |
| 3.6 | Modeling of bed shrinkage | 36 |
| 3.7 | Turbulence modeling | 39 |
| 3.8 | Radiation model | 41 |
| 3.9 | Physical Properties | 43 |
| 4. | Numerical solution for the packed bed model | 46 |
| 4.1 | Introduction to OpenFOAM | 46 |
| 4.2 | OpenFOAM solver | 47 |
| 4.3 | Introduction to Finite Volume method | 47 |
| 4.3.1 | Descritization of time | 48 |
| 4.3.2 | Descritization of space | 48 |
| 4.3.3 | Descritization of equations | 49 |
| 4.3.4 | Spatial descritization | 49 |
| 4.4 | Developed CFD solver using OpenFOAM | 51 |
| 4.4.1 | Initial and Boundary conditions | 53 |
| 4.4.2 | Computational mesh | 55 |
| 5. | Experimental set up and model validation | 56 |
| 5.1 | Model validation | 56 |

| | |
|---|----|
| 5.2 Optimization of air flow rate to the Gasifer based on CFD model | 63 |
| 5.3 Conclusion and future work | 65 |
| References | 66 |
| Appendix | 71 |



University of Moratuwa, Sri Lanka.
Electronic Theses & Dissertations
www.lib.mrt.ac.lk

LIST OF FIGURES

- Figure 1.1 Schematic diagram of fixed bed gasifiers.
- Figure 1.2 Main reaction zones of biomass packed bed in an Updraft Gasifier.
- Figure 2.1 Differential volume element located in flow domain and x momentum fluxes across its faces.
- Figure 2.2 Differential volume element located in flow domain and energy fluxes across its faces.
- Figure 2.3 Differential volume element located in flow domain and mass fluxes across its faces.
- Figure 2.4 Two step global pyrolysis scheme.
- Figure 2.5 Parallel pyrolysis scheme.
- Figure 2.6 Parallel pyrolysis scheme with tar decomposition.
- Figure 3.1 Computational domain of gasifier model
- Figure 3.2 Schematic diagram of mathematical model
- Figure 3.3 Energy transfer modes to wood particle
- Figure 3.4 Changes of governing equations as a result of bed shrinkage
- Figure 3.5 Motion of unit step variable z in the direction of bed shrinkage
- Figure 3.6 Schematic of Radiation model
- Figure 4.1 Structure of an OpenFOAM case
- Figure 4.2 A typical control volume in finite volume method
- Figure 4.3 Computational domain of the CFD solution
- Figure 4.4 File structure of developed OpenFOAM solver
- Figure 4.5 Solution Algorithm
- Figure 4.6 Computational mesh
- Figure 5.1 Schematic diagram of experimental laboratory scale gasification system
- Figure 5.2 Experimental laboratory scale gasification system
- Figure 5.3 Theoretical and experimental temperature profiles
- Figure 5.4 Theoretical and Experimental exit gas temperatures
- Figure 5.5 Theoretical and Experimental gas compositions after 60 minutes of ignition
- Figure 5.6 Development of reaction zones in the solution domain

- Figure 5.7 Variation of gas phase component volume fractions with time
- Figure 5.8 Bed reduction with time
- Figure 5.9 Temperature contours with in biomass bed after two hours from ignition.
- Figure 5.10 Gas phase velocity distribution.



University of Moratuwa, Sri Lanka.
Electronic Theses & Dissertations
www.lib.mrt.ac.lk

LIST OF TABLES

| | |
|-----------|---|
| Table 1.1 | Chemical reactions in a Gasifier |
| Table 2.1 | Kinetic rate expressions for homogenous reactions |
| Table 4.1 | Discretization Schemes. |
| Table 5.1 | Physical and chemical properties of fuel. |
| Table 5.2 | Simulation Results for different air flow rates |



University of Moratuwa, Sri Lanka.
Electronic Theses & Dissertations
www.lib.mrt.ac.lk

NOMENCLATURE

| | | | |
|----------------|--|-------------------|---|
| A | Specific surface area of packed bed (m^{-1}) | $r_{i,homo}$ | Rate of homogenous reaction i ($\text{Kg m}^{-3} \text{s}^{-1}$) |
| A_c | Specific surface area of char (m^{-1}) | $r_{m,i}$ | Mass transfer limited reaction rate ($\text{Kg m}^{-3} \text{s}^{-1}$) |
| A_d | Specific surface area for gas diffusion (m^{-1}) | $r_{k,i}$ | Kinetic reaction rate ($\text{Kg m}^{-3} \text{s}^{-1}$) |
| A_g | Cross sectional area of gasifier (m^2) | $r_{t,i}$ | Turbulent mixing limited reaction rate ($\text{kg m}^{-3} \text{s}^{-1}$) |
| A_j | pre-exponential factor for heterogeneous reactions ($\text{m s}^{-1} \text{T}^{-1}$) | Sh_j | Sherwood number for species j |
| A_r | Specific surface area available for radiation (m^{-1}) | S_\emptyset | Source term for property \emptyset |
| a | Absorption coefficient of gas phase (m^{-1}) | $S_{s,\emptyset}$ | Source term for property \emptyset due to solid phase |
| a_p | Absorption coefficient of solid phase (m^{-1}) | $S_{g,\emptyset}$ | Source term for property \emptyset due to gas phase |
| C_g | Heat capacity of gas phase ($\text{J kg}^{-1} \text{K}^{-1}$) | S_{ij} | Reynolds stress tensor (Pa) |
| C_s | Heat capacity of solid phase ($\text{J kg}^{-1} \text{K}^{-1}$) | T_g | Gas phase temperature (K) |
| $D_{i,g}$ | Diffusion coefficient of gas species i ($\text{m}^2 \text{s}^{-1}$) | $T_{g,in}$ | Inlet gas temperature (K) |
| d | Particle size of biomass (m) | T_s | Solid phase temperature (K) |
| E_i | Activation energy of reaction i (J mol^{-1}) | U_g | Gas phase velocity (m s^{-1}) |
| f_i | Pre-exponential factor of reaction i (s^{-1}) | $U_{g,in}$ | Inlet gas velocity (m s^{-1}) |
| G | Radiation intensity (W m^{-2}) | U_s | Shrinkage velocity (m s^{-1}) |
| h | Heat transfer coefficient ($\text{W m}^{-2} \text{K}^{-1}$) | v_i | Stoichiometric coefficient of species i |
| k | Turbulent kinetic energy ($\text{m}^2 \text{s}^{-2}$) | $Y_{i,g}$ | Mole fraction of gas species i |
| k_g | Thermal conductivity of gas phase ($\text{W m}^{-1} \text{K}^{-1}$) | $Y_{s,i}$ | Mole fraction of i in air |
| k_s | Thermal conductivity of solid phase ($\text{W m}^{-1} \text{K}^{-1}$) | $Y_{i,s}$ | Mole fraction of solid species i |
| $k_{m,j}$ | Mass transfer coefficient of species j (m s^{-1}) | σ | Stefan constant ($\text{W m}^{-2} \text{K}^4$) |
| M_i | Molecular weight of species i (kg mol^{-1}) | σ_p | Scattering coefficient of solid particles (m^{-1}) |
| m_i | Density of species i in a computational cell (kg m^{-3}) | ϵ | Emissivity of solid particles |
| Nu | Nusselt number | \emptyset | A general transport property |
| n | Refractive index of gas phase | ϵ_g | Gas phase fraction |
| Pr | Prandtl number | ϵ_s | Solid phase fraction |
| p | Pressure (Pa) | ρ_g | Density of gas phase (Kg m^{-3}) |
| p_{in} | Inlet pressure (Pa) | ρ_s | Density of solid phase (Kg m^{-3}) |
| Q_{rad} | Radiation heat source (W m^{-3}) | ρ_j | Cell density of species j (Kg m^{-3}) |
| Q_i | Initial heat source (W m^{-3}) | μ | Dynamic viscosity (Pa s) |
| Q_{sg} | Convective heat transfer rate (W m^{-3}) | $\sigma_{i,air}$ | Average collision diameter (A) |
| q_r | Radiation heat flux (W m^{-2}) | $\Omega_{i,air}$ | Diffusion collision integral |
| Re | Reynolds number | ϵ | Turbulent dissipation rate ($\text{m}^2 \text{s}^{-3}$) |
| $R_{g,pyro}$ | Rate of release of pyrolytic volatiles ($\text{Kg m}^{-3} \text{s}^{-1}$) | ΔH_i | Enthalpy of reaction i (J kg^{-1}) |
| r_i | Rate of reaction i ($\text{Kg m}^{-3} \text{s}^{-1}$) | \otimes | Vector outer product |
| $r_{i,hetero}$ | Rate of heterogeneous reaction i ($\text{Kg m}^{-3} \text{s}^{-1}$) | | |

LIST OF APPENDICES

| | | |
|----------|------------------------|----|
| Appendix | OpenFOAM Case Settings | 71 |
|----------|------------------------|----|



University of Moratuwa, Sri Lanka.
Electronic Theses & Dissertations
www.lib.mrt.ac.lk

Chapter 1

INTRODUCTION

1.1 Use of biomass as a renewable energy source

With the depletion of fossil fuels, worldwide research has been focused on finding alternative and renewable energy sources. Biomass is one of the major renewable energy sources of the present world accounting for nearly 10 -15 % of the current world's energy consumption [1]. It is expected to meet half of the world's primary energy consumption in future [2]. Presently, biomass is a widely used industrial energy source of Sri Lanka, which is used in tea, rubber and porcelain industries of the country. Sri Lanka has a large quantity of biomass reserves for energy generation. The waste from agricultural industry such as rice husks and hay can be turned into a valuable energy source for the country if efficient conversion methods were applied.

Biomass can be used in two main ways to produce energy in industry; direct combustion and conversion to a secondary fuel [3]. Direct biomass combustion can be observed in biomass boilers and furnaces. In which wood logs and wood chips are directly combusted to produce energy. In Sri Lankan tea industry, fire wood boilers are widely used to produce the heat required for tea drying process. The direct combustion of biomass has limited applications in process industry due to several drawbacks it introduces. One such problem is that direct combustion of biomass cannot produce high temperature flames required by certain applications and the versatility of biomass is also low. Because of these drawbacks, conversion of biomass into secondary fuels is gaining attention.

There are three main ways of conversion of biomass into secondary fuels; i.e thermo-chemical, bio-chemical and extraction processes [3],[4]. In thermo chemical conversion of biomass, biomass is cracked to constituent chemical compounds by application of heat. Gasification of biomass is one such thermal conversion process which is widely applied to produce a secondary fuel gas called Syngas. This gas is a mixture of carbon monoxide, carbon dioxide, hydrogen, methane, small amount of

light hydrocarbons and nitrogen [5],[6]. The gas produced is more versatile than original raw biomass fuel and can be used for a variety of applications. Examples are powering gas turbines, gas engines, as a fuel for high temperature furnaces. It can also be used as a raw material to produce liquid biofuels [6].

With a large amount of available biomass reserves, Sri Lanka has a good potential to utilize gasification technology to produce Syngas. However, this technology is still at the development stage and significant amount of research should be performed in the field to design efficient industrial scale gasifiers that will contribute to country's energy demand.

The present work contributes to this aim by developing a comprehensive numerical model for an updraft biomass gasifier, which can be used as a tool for design optimization of biomass gasifiers.

1.2 Biomass gasification

Gasification is a process by which biomass is partially oxidized at elevated temperatures to produce a combustible gas named Syngas or producer gas. The main reactions taking place in gasification process can be listed as follows [7], [8], [9], [10].

Table 1.1: Chemical reactions in a Gasifier

| <i>Heterogeneous reactions</i> | |
|--------------------------------|--|
| Pyrolysis of biomass | $Wood \rightarrow C + volatiles + Ash$ |
| Partial oxidation of biochar | $C + 0.5O_2 \rightarrow CO$ |
| Carbon dioxide gasification | $C + CO_2 \rightarrow 2CO$ |
| Water gasification | $C + H_2O \rightarrow CO + H_2$ |
| <i>Homogeneous reactions</i> | |
| Carbon monoxide oxidation | $CO + O_2 \rightarrow CO_2$ |
| Formation of water | $H_2 + O_2 \rightarrow H_2O$ |
| Methane oxidation | $CH_4 + 1.5O_2 \rightarrow CO + 2H_2O$ |
| Water gas shift reaction | $CO + H_2O \leftrightarrow CO_2 + H_2$ |

Biomass gasification can be classified according to gasification medium, gasifier type and configuration. Three main types of product gases based on calorific values can be obtained by varying these operational parameters [6]. The main gasification agents are: air, steam, air-steam mixture and oxygen-steam mixture [6]. The use of pure oxygen as the gasification medium is expensive and requires a complicated reactor, because of this, air is used. However, the nitrogen present in air dilute the product gas and air gasification can only produce outlet gases with low calorific values, usually between 4-6 MJ/Nm³. The pure oxygen gasification results in high quality gas with a calorific value of 10 – 18 MJ/Nm³. Oxygen-steam mixture can produce gases with a calorific value of 13 – 20 MJ/Nm³. Using hydrogen and hydrogenation can produce gases with significantly higher calorific values of around 40 MJ/Nm³ [6].

1.3 Gasifier types

Gasifiers can be classified as fluidized bed gasifiers and fixed bed gasifiers. Fixed bed gasifiers vary in configuration, major configurations are updraft, downdraft and cross flow gasifiers and are simpler in design [6]. Schematics of these gasifiers are illustrated in Figure 1. Fluidized bed gasifiers can be classified as circulating fluidized bed gasifiers and bubbling bed gasifiers. About 75% of the energy content of the initial biomass fuel can be recovered from the produced gas in packed bed gasifiers. The energy loss is mainly because of the heat loss due to sensible heat carried away by the product gases and radiation losses. The typical composition of the produced Syngas in a fixed bed gasifier operated with air is: 45-55 % Nitrogen, less than 10% hydrogen, 15-20% carbon monoxide, 15-20% carbon dioxide and less than 5% methane [6].

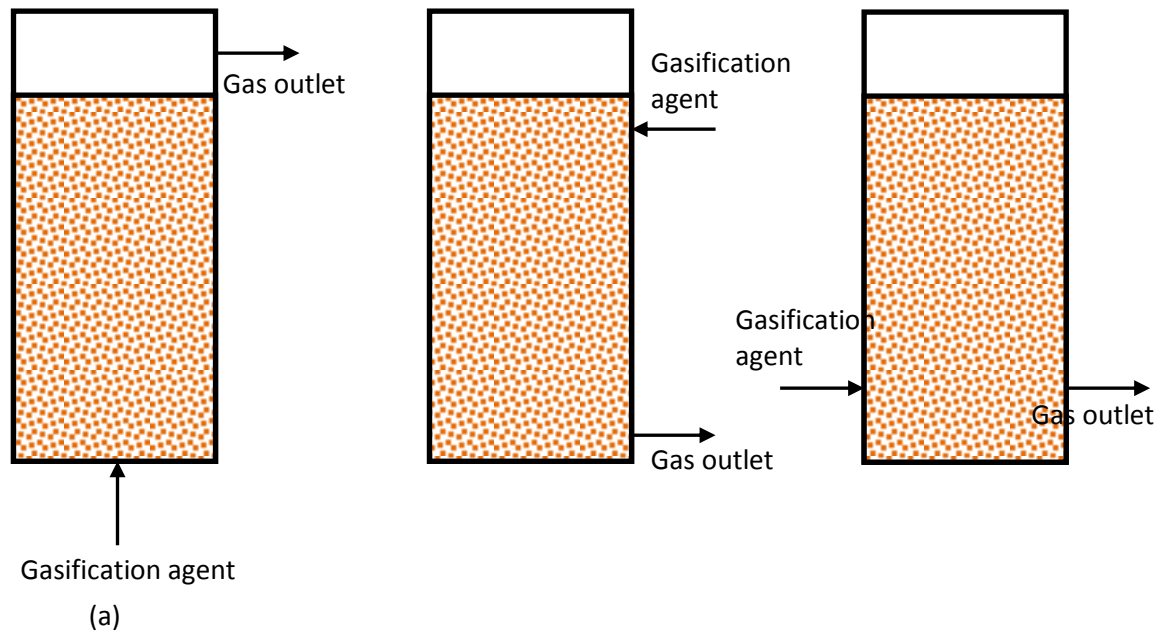


Figure 1.1: Schematic diagram of fixed bed gasifiers. (a) Updraft (b) Down draft (c) Cross flow

1.3.1 Fixed bed gasifiers

1.3.1.1 Updraft gasifiers

In updraft gasifiers, biomass feed is introduced from the top of the gasifier and gasifying medium is introduced from the bottom through a grate. Four regions can be identified during the operation of these gasifiers [8]. Immediately above the grate, where oxygen is abundant, combustion reactions take place and biomass is combusted to produce heat. This zone is called the combustion zone. Above the combustion zone, where oxygen concentration of the gasifying medium is low, bio char produced as a result from the heat generated from the combustion zone is gasified. This zone is called the gasification zone. The main reactions taking place in this zone are carbon dioxide gasification and steam gasification. Above the gasification zone the biomass conversion into char takes place as a result of heat generated by lower regions. This zone is called the pyrolysis zone. In the topmost layer of the packed bed, temperatures are low for pyrolysis process to initiate. In this

zone, moisture of the biomass is evaporated and biomass is dried. This region is termed the drying zone. These zones are illustrated in Figure 1.2. The temperature of the producer gas produced in updraft gasifiers is considerably low, making the overall energy efficiency of the gasifier high.

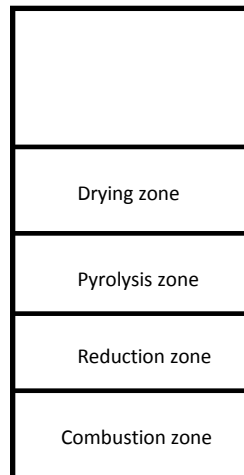


Figure 1.2: Main reaction zones of biomass packed bed in an Updraft Gasifier

1.3.1.2 Downdraft gasifiers

In downdraft gasifiers, air is introduced from a side of the packed bed and moves in downward direction. The reaction zones are similar to that of an updraft gasifier expect the location of combustion and gasification zones are altered. The gasification zone becomes the lowest layer with combustion zone on top of it [7]. Because of the high temperatures of the outlet zone, the temperature of the gas leaving the gasifier is high. This reduces the overall energy efficiency of downdraft gasifiers. Because the outlet is nearer to the combustion zone, the particulate matter in the outlet gas is also high. However, the movement of the gases through the hot gasification zone allows the partial cracking of tar formed during gasification. This results in a gas with low tar content [6].

1.3.1.3 Cross-flow gasifiers

In cross flow gasifiers, air is introduced at the side of the packed bed and withdrawn from the opposite side at the same level [6], [7]. The gases leaving the gasifier are at a high temperature, making the efficiency of the process low.

1.3.2 Parameters affecting the quality of the produced gas

The composition of the produced gas depends on many parameters. These include; gasifying medium, gasifier type, properties of biomass, moisture content, particle size, temperature of the gasification zone, operating pressure, equivalence ratio [5]. For a given gasifier, two main parameters determine the quality of the produced gas. These parameters are gasification temperature and equivalence ratio. As temperature of the gasification zone increases, the hydrogen content of the Syngas increases while Carbon monoxide, Carbon dioxide and other gas concentrations decrease [5].

The gasifier equivalence ratio is defined as the amount of oxygen supplied to the gasifier divided by the amount of oxygen needed for the complete combustion. Studies have shown that higher equivalence ratios results in poor gas quality. This is because when equivalence ratio increases complete combustion of biomass is favored. The most effective value of equivalence ratio for a given process depends on several other factors as well, these factors include, gasifier configuration and fuel type. It has been observed that for downdraft gasifiers operated with wood, equivalence ratio between 0.3-0.35 produce outlet gases with low calorific values of around 1000 kcal Nm⁻³. Some researchers have investigated the performance of updraft gasifiers under various operating conditions and have found that an equivalence ratio of 0.25 gave the best performance [5]. However these values are very sensitive to the properties of the feedstock and gasifier geometry.

The moisture present in the biomass feed affects the composition of the Syngas as well as the operation of the gasifier. Presence of excessive moisture in biomass reduces the overall energy efficiency of the system, because a large amount of energy is used to evaporate the moisture present in biomass. Also it has been found that the carbon monoxide content of the Syngas is high when biomass moisture content is low. Higher moisture contents increase the carbon dioxide fraction of the produced gas, thus reducing its quality. High moisture contents reduce the temperature achieved in the oxidation zone as well, this results in incomplete cracking of pyrolysis products [6]. Typically biomass moisture content should be lowered to a value between 10-15% dry basis before feeding it to the gasifier. This

value may change according to the other operational parameters. This requirement of pre-drying introduces significant energy costs to the process.

The suitable particle size of the feed material depends on the geometry of the gasifier. Larger particle sizes can prevent the feed from moving downwards and smaller particles can result in closely packed conditions, causing higher pressure drops [6].

Another factor that affects the quality of the produced gas is superficial velocity. It is defined to be equal to gas flow rate divided by the cross sectional area of the gasifier. Low values of superficial velocity results in slow pyrolysis of biomass with a higher yield of char. Higher superficial velocities reduces the efficiency of tar cracking process [5]. The superficial velocity affects the final compositions of the combustible components in the outlet gas, and is therefore an important operating parameter.

1.4 Computational fluid dynamics modeling as a tool to optimize biomass gasifiers

As described in the previous section, a number of factors determine the quality of the produced gas of a gasifier. In most cases, these factors are dependent on each other, for an example, the optimum value of the equivalence ratio depends on the gasifier type and properties of the feed material. This dependence makes the process optimization of gasifiers difficult. Usually the data published on literature are for a specific gasifier configuration and feed material. Using such data to control the performance of a gasifier operated with a different feed will produce poor results. This makes the design of gasifiers very specific to the feed material, geometry and configuration. The values present in the literature can only be used as guidelines and optimum values should be found for the case at hand. This can be done in two main ways. One is the experimental approach and the other is through computer aided simulations. Experimental approach follows a series of experiments, usually on scaled down laboratory scale gasifiers [12], [13], [14]. Parameters such as the optimum equivalence ratio can be determined by measuring the gas quality under various equivalence ratios until the best results are obtained. However, experimental approach introduces a series of difficulties and drawbacks. It is very difficult to



perform experimental analysis on pilot scales systems, especially when considering geometry optimization, therefore scaled down models have to be used for experimental analysis. The results obtained on scaled down systems may not fully work on the pilot scale system. The scale down systems cannot be used to determine the effects of biomass particle sizes, as particle size relies on the diameter of the real system. Scaling down the particle size will not produce equivalent results because the packing factors will differ between the two systems. Also, taking measurements inside packed beds is a difficult task considering the higher temperatures present in an operational gasifier [15]. Because of these reasons, the experimental approach is usually difficult, time consuming, costly and the accuracy of the results are also low.

Therefore many researchers use the computer based approach to analyze packed bed processes. A large number of research works are available in literature where numerical models are used to optimize packed bed processes [2], [11], [16], [17], [18]. Mathematical models offer certain advantages over the conventional experimental procedure. Mathematical models can produce a large number of data points as compared to fewer experimental data, for example, when measuring temperature experimental analysis can provide temperatures at only a finite number of locations along the packed bed, while numerical models can provide the complete variation of the temperature profile over the region of interest. These models can be used to analyze spatial distributions of variables with in the reactor [19]. With the development of the computer hardware technology, computational fluid dynamics (CFD) is widely applied as a numerical modeling tool. CFD models can be made to match the exact geometry of the real scale gasifier, as a result no scaling down problems arise, in CFD simulations, any number of input parameters can be easily changed at will, including equivalence ratio, particle size, moisture content, feed properties, superficial velocity etc. and results can be obtained. To do such an analysis using experimental approach will require a serious effort and a large amount of time and resources. CFD simulations are best suited to perform geometry optimization. A large number of geometrical parameters can be optimized by simply changing the computational mesh. Because of these advantages CFD models are now

widely used by researchers around the world as a tool to study and optimize gasification process [7], [11], [16], [20].

1.5 Objectives of present research

The present research is focused on two main objectives.

- Study the thermo-chemical processes in an updraft biomass gasifier.
- Develop a comprehensive computational fluid dynamics model for an updraft biomass gasifier and use this model for optimization of operational parameters of a pilot scale gasifier.

1.6 A summary of the presented research

In the present work a two dimensional real-time two phase CFD model has been developed for an updraft biomass packed bed gasifier. The model uses inlet air at room temperature as the gasifying medium and a fixed batch of biomass. The biomass batch is initially ignited by a heat source which is removed after a certain amount of time. And the presented mathematical model is capable of maintaining the operation by the own heat emitted by combustion reactions, until the model is finished, as in the real world scenario. Since the operation is batch wise, model is transient and takes into consideration the effect of bed movement as a result of shrinkage. The model is capable of tracking the movement of interface between solid packed bed and gas free board. The two phase model is developed using the Euler-Euler approach. The model consists of several sub models, including reaction models which govern the reaction rates and compositions of the products, turbulence model for packed bed gas phase and free board, a radiation model for solid phase, a bed shrinkage model, and interphase heat transfer models. A novel low temperature drying model was developed and applied to predict drying rates in the range of 300 to 473 K. This drying model was simulated using MATLAB-Simulink simulation tool and validated using experimental data for wood chip drying. The final mathematical model for the gasifier is converted into a numerical model using open source CFD tool OpenFOAM. A new code was developed using C++ language and available tools in OpenFOAM package to include all the relevant differential equations and procedures

in the mathematical model. To validate the CFD model, simulation results are compared against experimental data from an operational laboratory gasifier. It is found that the model is in good agreement with experimental data.

The following list summarizes the input parameters of the developed model. These parameters can be changed at run time. So the presented model can be used to optimize all of these parameters for a given gasifier.

Input parameters of the developed model

Solid properties

- Particle size
- Packed bed porosity
- Density of the biomass feed
- Heat capacity polynomial coefficients
- Emission characteristics of the feed biomass as obtained by ultimate and proximate analysis
- Initial dry basis moisture content
- Fiber saturation value of the biomass species
- Pyrolysis activation energy and pre exponential factor of the feed biomass
- Initial packed bed height

Gas properties

- Gas inlet velocity
- Inlet gas composition
- Inlet gas temperature
- Inlet gas density
- Relative humidity of the inlet gas
- Inlet gas pressure
- Turbulent properties of the inlet gas stream

Chapter 2

REVIEW OF PACKED BED MODELS

2.1 Modeling approaches

Numerical models for gasification process have been developed by many researchers over the years. These models vary in complexity from very simple ones to sophisticated models describing various phenomena occurring inside the reactor. These models can be classified in various ways. Mainly, the models can be classified depending on the dimensionality, resolution of the model and method of inclusion of reaction kinetics [1], [21]. When classifying dimensionally, the models can be classified into three categories; one dimensional models, two dimensional models and three dimensional models. One dimensional models describe variation of parameters along the bed height only [2]. These models assume that the flow through the gasifier can be treated as a plug flow. These models can be used to derive axial temperature profiles and compositions of the outlet gases. But they cannot be used to predict the effects of geometry variations of the gasifier and as a result not suitable to design optimization work. Two dimensional models consider the variation of process variables in axial and radial directions of the gasifier [1], [11]. Since most gasifiers are axisymmetric in geometry, these models provide a good description of real world scenario. Two dimensional models can be used to study the effects of symmetric geometry changes of the design. Three dimensional models, which are very rare in literature and are computationally very costly, consider variations of the fields in all three directions and are the most accurate model class [15]. However, their use is limited due to the computational cost involved as compared to the two dimensional models, which provide good results in symmetric cases. Three dimensional models are useful when analyzing non symmetric phenomena such as channeling within the packed bed.

The other method of classification is by resolution of the model. The gasification process consists of a multiphase system of solid and gas phases. Models can be

classified according to the way these two phases are mathematically treated. Three main classifications can be identified from the literature. These are: single particle models, two fluid models and Euler-Lagrange models. Single particle models describe the drying, pyrolysis, combustion and gasification of a single biomass block [9], [22]. These models cannot be applied to packed bed processes. These models are usually highly comprehensive and take into consideration the mechanisms of internal species transport, various anisotropies of the physical properties of the wood, such as anisotropy in diffusion coefficients [18], [23]. They are very accurate in describing the thermal conversion process of a single biomass particle. The two fluid models or the Euler-Euler models are the most common modeling approach used to model packed bed processes. In this method, biomass packed bed is considered as a continuous porous media, consisting of a solid phase (biomass) and a gas phase [24]. Both the gas and solid phases are treated as fluids and when deriving the governing transport equations, a volume of fluid approach based on the value of porosity is used. These models are computationally less costly and provide a good description of packed bed process. However, these models neglect the internal processes occurring within the solid particles, and therefore accurate only when the particles of the packed bed can be considered thermally thin [21]. This assumption is usually valid for packed beds of small wood chips and straw [21]. The Euler-Lagrange models treat solid and gas phases separately. In this approach gas phase is modeled as a continuous fluid and the solid phase is considered as a sum of individual particles. All the interactions among the particles are considered. Equations are solved for each particle separately and combined to get the final result [15], [25], [26]. Though this approach is highly accurate, it demands high computing facilities and longer times to simulate, because biomass packed bed consists of large number of separate particles. A limited number of these models exist in literature.

Mathematical models can also be classified according to the way chemistry is treated. There are two classes of models: equilibrium models and kinetic models [27]. Equilibrium models are based on chemical equilibrium of the process and the results of the computations based on equilibrium models do not often agree with the actual experimentally observed gas compositions at the exit of the gasifier [11].

Kinetic models are developed based on the chemical kinetics of the reactions taking place inside the gasifier. The kinetic rates of reactions are obtained from experimentally determined correlations and these models are often highly coupled with transport phenomena of the process [2], [8], [11]. This is mainly because reactions rates in combustion processes are often controlled by diffusion and homogenous reaction rates are controlled by turbulent mixing [1]. Kinetic models produce better results that are closer to experimentally observed values as compared to equilibrium models.

2.2 Governing transport equations

In order to obtain the distribution of variables of interest (gas molar fractions, temperatures, pressure distribution, velocity distribution) an equation governing their distributions need to be solved. These equations are called the governing transport equations. The governing transport equation for a general scalar quantity ϕ is obtained by considering the conservation of ϕ over a differential volume element of the solution domain. In following sections governing transport equations for momentum, temperature and pressure are obtained for a single phase system.

2.2.1 Momentum conservation equation

The momentum conservation equation is derived by applying the momentum balance in each coordinate direction to the differential volume element shown in the Figure 2.1.

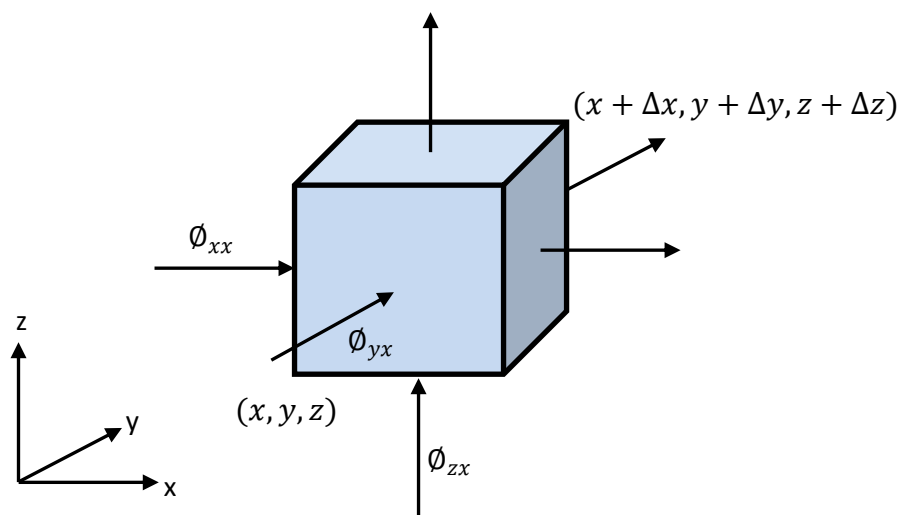


Figure 2.1: Differential volume element located in flow domain and x momentum fluxes across its faces.

The momentum balance can be written as [28],

Rate of increase of momentum = rate of momentum in – rate of momentum out
+ external force

The fluxes of x momentum are shown in Figure 2.1

ϕ_{ij} is the combined momentum flux tensor which can be interpreted as the flux of j momentum in i direction.

Based on these fluxes, the total rate of x momentum into the fluid element can be written as,

$$(\phi_{xx})|_x \Delta y \Delta z + (\phi_{yx})|_y \Delta x \Delta z + (\phi_{zx})|_z \Delta x \Delta y$$

And the total rate of x momentum out of the system is equal to,



$$(\phi_{xx})|_{x+\Delta x} \Delta y \Delta z + (\phi_{yx})|_{y+\Delta y} \Delta x \Delta z + (\phi_{zx})|_{z+\Delta z} \Delta x \Delta y$$

The external gravitational force on the fluid element in x direction is given by,

$$\rho g_x \Delta x \Delta y \Delta z$$

Substituting these expressions in the momentum balance relation results in,

$$\begin{aligned} \Delta x \Delta y \Delta z \frac{\partial}{\partial t} \rho U_x &= \Delta y \Delta z ((\phi_{xx})|_x - (\phi_{xx})|_{x+\Delta x}) + \Delta x \Delta z ((\phi_{yx})|_y - (\phi_{yx})|_{y+\Delta y}) \\ &+ \Delta x \Delta y ((\phi_{zx})|_z - (\phi_{zx})|_{z+\Delta z}) \\ &+ \rho g_x \Delta x \Delta y \Delta z \end{aligned} \quad (2.1)$$

Dividing the entire equation by $\Delta x \Delta y \Delta z$ and re arranging,

$$\begin{aligned} & \frac{\partial}{\partial t} \rho U_x \\ &= - \frac{(\phi_{xx})|_{x+\Delta x} - (\phi_{xx})|_x}{\Delta x} - \frac{(\phi_{yx})|_{y+\Delta y} - (\phi_{yx})|_y}{\Delta y} - \frac{(\phi_{zx})|_{z+\Delta z} - (\phi_{zx})|_{z+\Delta z}}{\Delta z} \\ &+ \rho g_x \end{aligned} \quad (2.2)$$

Taking the limit as Δx , Δy , Δz go to zero, results in the following partial differential equation for the x component of velocity,

$$\frac{\partial}{\partial t} \rho U_x = - \left(\frac{\partial}{\partial x} \phi_{xx} + \frac{\partial}{\partial y} \phi_{yx} + \frac{\partial}{\partial z} \phi_{zx} \right) + \rho g_x \quad (2.3)$$

By similarly considering the fluxes in other directions, equations for y and z momentum can be derived as expressed below.

$$\frac{\partial}{\partial t} \rho U_y = - \left(\frac{\partial}{\partial x} \phi_{xy} + \frac{\partial}{\partial y} \phi_{yy} + \frac{\partial}{\partial z} \phi_{zy} \right) + \rho g_y \quad (2.4)$$

$$\frac{\partial}{\partial t} \rho U_z = - \left(\frac{\partial}{\partial x} \phi_{xz} + \frac{\partial}{\partial y} \phi_{yz} + \frac{\partial}{\partial z} \phi_{zz} \right) + \rho g_z \quad (2.5)$$

For a general coordinate direction i , these equations can be written as

$$\frac{\partial}{\partial t} \rho U_i = -[\nabla \cdot \phi]_i + \rho g_i \quad (2.6)$$

Where $\nabla \cdot \phi$ represents the contraction of the second order momentum flux tensor with the differential operator $\frac{\partial}{\partial x^i}$

Combining the separate equations for each coordinate direction, the final vector form of the momentum equation can be written as,

$$\frac{\partial}{\partial t} \rho \mathbf{U} = -[\nabla \cdot \phi] + \rho \mathbf{g} \quad (2.7)$$

The combined momentum flux tensor ϕ is given by,

$$\phi = \rho \mathbf{U} \otimes \mathbf{U} + p \delta + \boldsymbol{\tau} \quad (2.8)$$

Where δ is the kroneker delta symbol and τ is the molecular momentum flux tensor.

For a Newtonian fluid, τ is given by Newton's law of viscosity,

$$\tau = -\mu \nabla U \quad (2.9)$$

Substituting these relations into equation x, results in the transport equation for velocity,

$$\frac{\partial}{\partial t} \rho U = -\nabla \cdot (\rho U \otimes U) - \nabla p + \mu \nabla \cdot \nabla U + \rho g \quad (2.10)$$

For a gas flow, the gravitational force can be neglected compared to other terms present in the equation, therefore the final governing equation for the gas phase velocity is,

$$\frac{\partial}{\partial t} \rho U + \nabla \cdot (\rho U \otimes U) - \mu \nabla \cdot \nabla U = -\nabla p \quad (2.11)$$



University of Moratuwa, Sri Lanka.
Electronic Theses & Dissertations

2.2.2 Temperature equation

The governing equation for temperature is obtained by considering the energy balance for a differential volume element as shown in Figure 2.2,

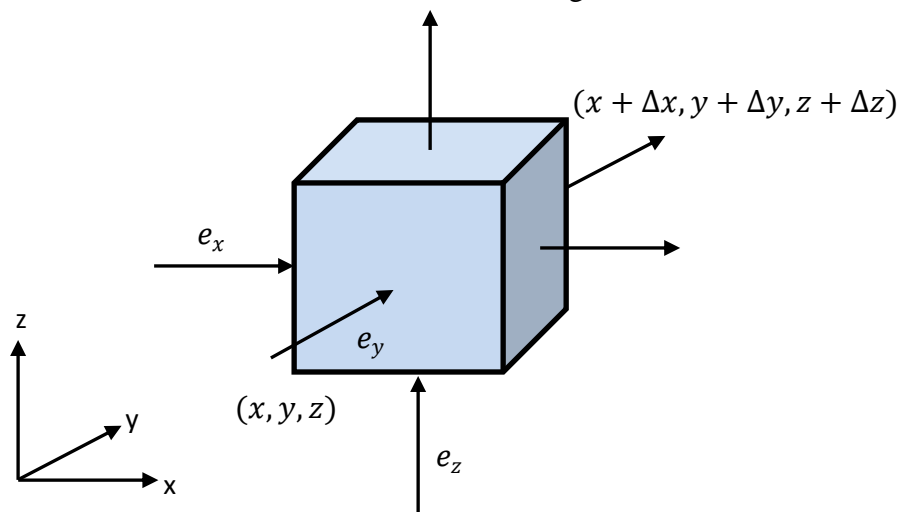


Figure 2.2: Differential volume element located in flow domain and energy fluxes across its faces.

The energy balance can be written as [28],

Rate of increase of energy = rate of energy in – rate of energy out + sources

The rate at which energy enters the fluid element in all three directions can be written as,

$$e_x|_x \Delta y \Delta z + e_y|_y \Delta x \Delta z + e_z|_z \Delta x \Delta y$$

Where e is the energy flux vector of the fluid,

The rate at which energy flows out of the fluid element is equal to,

$$e_x|_{x+\Delta x} \Delta y \Delta z + e_y|_{y+\Delta y} \Delta x \Delta z + e_z|_{z+\Delta z} \Delta x \Delta y$$

Substituting these quantities in energy balance results in,

$$\begin{aligned} & \Delta x \Delta y \Delta z \frac{\partial}{\partial t} \left(\frac{1}{2} \rho U^2 + \rho \hat{U} \right) \\ & = (e_x|_x + e_x|_{x+\Delta x}) \Delta y \Delta z + (e_y|_y + e_y|_{y+\Delta y}) \Delta x \Delta z + (e_z|_z + e_z|_{z+\Delta z}) \Delta x \Delta y \\ & + \Delta x \Delta y \Delta z S \end{aligned} \quad (2.12)$$

Dividing by $\Delta x \Delta y \Delta z$ and re arranging gives,

$$\begin{aligned} & \frac{\partial}{\partial t} \left(\frac{1}{2} \rho U^2 + \rho \hat{U} \right) \\ & = - \frac{e_x|_{x+\Delta x} - e_x|_x}{\Delta x} - \frac{e_y|_{y+\Delta y} - e_y|_y}{\Delta y} - \frac{e_z|_{z+\Delta z} - e_z|_z}{\Delta z} + S \end{aligned} \quad (2.13)$$

Taking the limit as $\Delta x, \Delta y, \Delta z$ go to zero results in the following partial differential equation for enthalpy.

$$\frac{\partial}{\partial t} \left(\frac{1}{2} \rho U^2 + \rho \hat{U} \right) = - \left(\frac{\partial e_x}{\partial x} + \frac{\partial e_y}{\partial y} + \frac{\partial e_z}{\partial z} \right) + S \quad (2.14)$$

In vector notation, this can be written as,

$$\frac{\partial}{\partial t} \left(\frac{1}{2} \rho U^2 + \rho \hat{U} \right) = -\nabla \cdot e + S \quad (2.15)$$

The energy flux vector, e can be written as [28],

$$e = \left(\frac{1}{2} \rho U^2 + \rho \hat{U} \right) U + [\tau \cdot U] + pU + q \quad (2.16)$$

Substituting this expression in equation 2.15 results in,

$$\frac{\partial}{\partial t} \left(\frac{1}{2} \rho U^2 + \rho \hat{U} \right) = -\nabla \cdot \left(\frac{1}{2} \rho U^2 + \rho \hat{U} \right) U - \nabla \cdot [\tau \cdot U] - \nabla \cdot pU - \nabla \cdot q + S \quad (2.17)$$

This equation can be further simplified using the equation of mechanical energy of a fluid, obtained by taking the dot product of velocity vector with momentum conservation equation.

$$\frac{\partial}{\partial t} \left(\frac{1}{2} \rho U^2 \right) = -\nabla \cdot \frac{1}{2} \rho U^2 U - \nabla \cdot pU + p \nabla \cdot U - \nabla \cdot [\tau \cdot U] + \tau : \nabla U \quad (2.18)$$

Where : represent the double inner product of the two second order tensors τ and ∇U .

Substituting equation 2.18 in 2.17 and simplifying results in the following equation for the specific internal energy of the fluid,

$$\frac{\partial}{\partial t} (\rho \hat{U}) = -\nabla \cdot \rho \hat{U} U - \nabla \cdot q - p \nabla \cdot U - \tau : \nabla U + S \quad (2.19)$$

For a perfect gas [29],

$$\hat{U} = C_v T \quad (2.20)$$

Substituting for internal energy in equation 2.19 and re arranging,

$$\frac{\partial \rho C_v T}{\partial t} + \nabla \cdot \rho C_v T U + \nabla \cdot q = -p \nabla \cdot U - \tau : \nabla U + S \quad (2.21)$$

By defining the source term as,

$$S_T = S - p\nabla \cdot \mathbf{U} - \tau : \nabla \mathbf{U} \quad (2.22)$$

The energy equation can be written,

$$\frac{\partial \rho C_v T}{\partial t} + \nabla \cdot \rho C_v T \mathbf{U} + \nabla \cdot \mathbf{q} = S_T \quad (2.23)$$

Finally, \mathbf{q} can be expressed in Fourier's law for heat conduction by [28],

$$\mathbf{q} = -k\nabla T \quad (2.24)$$

Substituting this in equation 2.23 gives the transport equation for temperature of the fluid.

$$\frac{\partial \rho C_v T}{\partial t} + \nabla \cdot \rho C_v T \mathbf{U} - \nabla \cdot (k\nabla T) = S_T \quad (2.25)$$

2.2.3 Species conservation equations

The transport equation for each species is obtained by considering the mass balance of respective species over an elemental volume as shown in Figure 2.3.

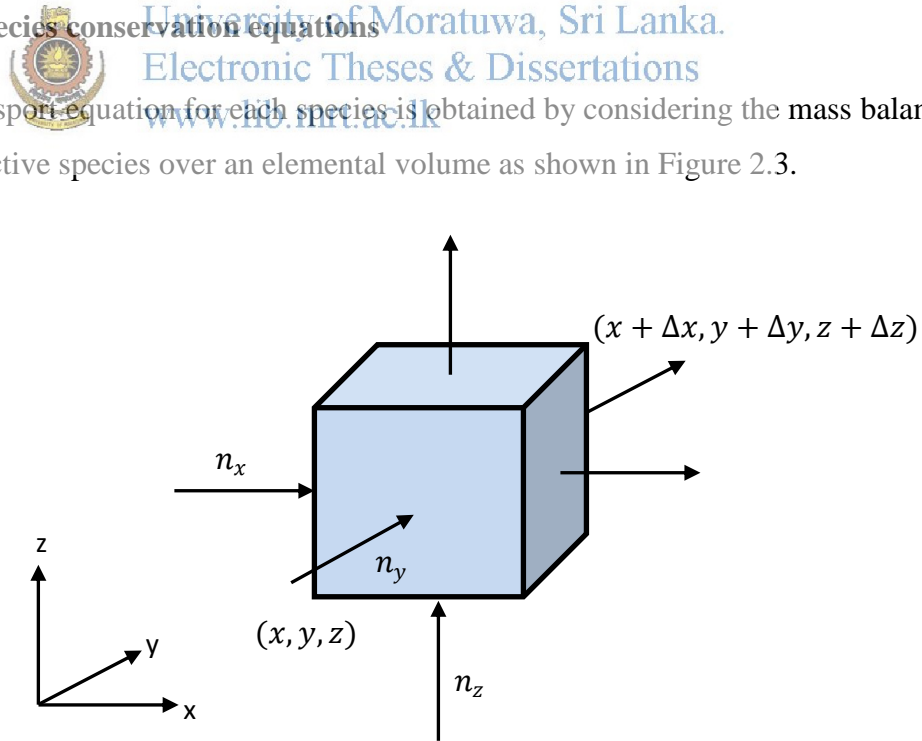


Figure 2.3: Differential volume element located in flow domain and mass fluxes across its faces.

Mass balance equation can be written as [28],

Rate of increase of mass of species i = Rate of mass in – Rate of mass out + source

The rate of mass of species i into the volume element is equal to,

$$n_i|_x \Delta y \Delta z + n_i|_y \Delta x \Delta z + n_i|_z \Delta x \Delta y$$

Where n_i is the mass flux vector of the i^{th} species.

Rate of mass of species i out of the control volume can be written as,

$$n_i|_{x+\Delta x} \Delta y \Delta z + n_i|_{y+\Delta y} \Delta x \Delta z + n_i|_{z+\Delta z} \Delta x \Delta y$$

Substituting these expressions into mass balance equation results in,

$$\begin{aligned} & \Delta x \Delta y \Delta z \frac{\partial}{\partial t} (\rho Y_i) \\ &= (n_i|_x - n_i|_{x+\Delta x}) \Delta y \Delta z + (n_i|_y - n_i|_{y+\Delta y}) \Delta x \Delta z + (n_i|_z - n_i|_{z+\Delta z}) \Delta x \Delta y \\ &+ \Delta x \Delta y \Delta z r_i \end{aligned} \quad (2.26)$$

Where r_i is the rate of generation of i through chemical reactions.



University of Moratuwa, Sri Lanka.
Electronic Theses & Dissertations
www.lib.mrt.ac.lk

Dividing by $\Delta x \Delta y \Delta z$ and re arranging results in,

$$\frac{\partial}{\partial t} (\rho Y_i) = -\frac{n_i|_{x+\Delta x} - n_i|_x}{\Delta x} - \frac{n_i|_{y+\Delta y} - n_i|_y}{\Delta y} - \frac{n_i|_{z+\Delta z} - n_i|_z}{\Delta z} + r_i \quad (2.27)$$

Taking the limit as $\Delta x, \Delta y, \Delta z$ go to zero results in the following partial differential equation,

$$\frac{\partial}{\partial t} (\rho Y_i) = -\left(\frac{\partial n_i}{\partial x} + \frac{\partial n_i}{\partial y} + \frac{\partial n_i}{\partial z}\right) + r_i \quad (2.28)$$

In vector notation, above equation can be written as,

$$\frac{\partial}{\partial t} (\rho Y_i) = -\nabla \cdot n_i + r_i \quad (2.29)$$

The mass flux vector n_i , consists of convective and diffusive mass transfer terms and is equal to [28],

$$n_i = j_i + \rho_i U \quad (2.30)$$

Where ρ_i is the density of the i^{th} species and j_i is the diffusive flux of i^{th} species.

j_i is given by Fick's law of molecular diffusion according to [28],

$$j_i = -\rho D_i \nabla Y_i \quad (2.31)$$

Using above expression, n_i can be written as,

$$n_i = -\rho D_i \nabla Y_i + \rho Y_i U \quad (2.32)$$

Substituting in equation x and re arranging gives the governing transport equation for the species mole fraction Y_i

$$\frac{\partial}{\partial t}(\rho Y_i) + \nabla \cdot (\rho Y_i U) - \nabla \cdot (\rho D_i \nabla Y_i) = r_i \quad (2.33)$$

2.3 Reaction rate models



University of Moratuwa, Sri Lanka.
Electronic Theses & Dissertations
www.lib.mrt.ac.lk

In order to evaluate the source terms present in governing equations derived in the previous section, rates of the chemical and thermal processes in gasifier should be known. These rates depend on many factors, such as chemical kinetics, diffusion rates of gas species, porosity of biomass particles. In order to obtain accurate expressions for reaction rate and source terms, an understanding of chemical and thermal processes is required. This section reviews the four important processes in a gasifier and modeling approaches used to model these processes.

The main chemical processes in a gasification process are [8]:

- Drying
- Pyrolysis
- Reduction
- Combustion

In mathematical modeling of a gasifier, these processes are included in the mathematical model as rate terms in transport equations. Because of this, in modeling view point, the most important parameter of these processes is the rate of the process. A number of different models are available for describing the rate of each of these processes. These models are described in following sections.

2.4 Drying

Drying is the removal of moisture from raw biomass fuel by absorption of heat from the environment. As described in Chapter 1, the moisture content directly affects the thermal efficiency of a gasifier. Also, some chemical reactions in the gasification process involve moisture present in the gas phase, for a gasifier operated using air, as in the present case, the main source of gas phase moisture is the drying process. The evolution of biomass moisture is solely governed by drying rate. Therefore, accurate modeling of drying process is important for successful modeling of gasification process. Two types of major drying models are used in literature to obtain expressions for drying rates. They are first order kinetic models and equilibrium models [21].

2.4.1 First order kinetic model

This is the most common model used to describe drying in literature and are used by researchers in simulating gasification process [8][24]. The model expresses drying rate by an Arrhenius type equation given by,

$$r_d = A \exp\left(\frac{-E_d}{RT_s}\right) \rho_{moisture} \quad (2.34)$$

2.4.2 Equilibrium model

These models are based on the assumption that water vapour is in equilibrium with liquid water. The rate is expressed as proportional to the driving force developed as a result of moisture deference at biomass particle surface and surrounding gas stream [30][31]. The rate equation in equilibrium model is given by,

$$r_d = kA(\rho_{m,surface} - \rho_{m,gas}) \quad (2.35)$$

In kinetic models it is difficult to incorporate the effects of external factors such as air flow rate, air humidity and wood properties such as density, thermal conductivity, heat capacity and particle size on drying process. This limits the accuracy and scope of the final model because the model cannot be used to predict the impact of above mentioned properties on efficiency of conversion process. They can be applied for high temperature drying processes [8]. Equilibrium models can be used to consider these effects through the value of mass transfer coefficient k. They are however applied for predicting low temperature drying rates. In the present work, a drying model is developed for low temperatures which incorporate the effects of particle properties and air flow on the drying process. This is discussed further in chapter 3. For higher temperatures, drying rate is modeled by equation 2.34.

2.5 Pyrolysis

Pyrolysis is the thermal decomposition of biomass into volatile gases and char. Pyrolysis in wood is usually initiated at 473 K [10]. The basic phenomena that take place during pyrolysis are heat transfer from a heat source leading to an increase in fuel temperature, initiation of pyrolysis reactions due to this increased temperature and reduction of biomass into volatiles and char. Pyrolysis is an important step in gasification process because products of pyrolysis process are the reactants of all the other chemical processes that take place in the system. The decomposition of wood as a result of pyrolysis involves a complex series of reactions, taking place in different pathways. These pathways may depend on heating conditions and biomass species. This complexity of pyrolysis phenomenon has presented a considerable challenge in developing mathematical models for pyrolysis process.

The basic constituents of wood are cellulose, hemicellulose and lignin[32]. The products of pyrolysis are a combination of products obtained by separate pyrolysis of each of the basic constituents. The main products of cellulose pyrolysis are char, tar and gaseous products. Hemicellulose mainly decomposes into more volatiles and produces a lower amount of char and tar. The main product of Lignin pyrolysis is

char. The pyrolysis of wood can be separated into two steps: Primary pyrolysis and secondary pyrolysis. Primary pyrolysis is the decomposition of basic constituents of wood and during secondary pyrolysis, the products formed in primary pyrolysis is further decomposed [10][32]. Hemicellulose decomposes when temperature of wood is in the range of 473 K to 553 K, releasing volatiles, mainly carbon monoxide and carbon dioxide. From 553 K to 593 K, the decomposition of cellulose takes place, again releasing volatiles, when temperature exceeds 593 K, Lignin decomposes, mainly forming carbon.

For modeling purposes, pyrolysis process is represented by simplified reaction schemes. Various researchers have developed different reaction schemes of varying complexity [2][10][11][32]. Some of these schemes are illustrated in following section.

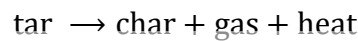


Figure 2.4: Two step global pyrolysis scheme
 University of Moratuwa, Sri Lanka
 Electronic Theses & Dissertations
 www.lib.mrt.ac.lk

Above reactions describe a pyrolysis model of two step global reactions. During first step biomass decomposes into char, tar and volatiles. During second stage, decomposition of tar into char and volatiles take place.

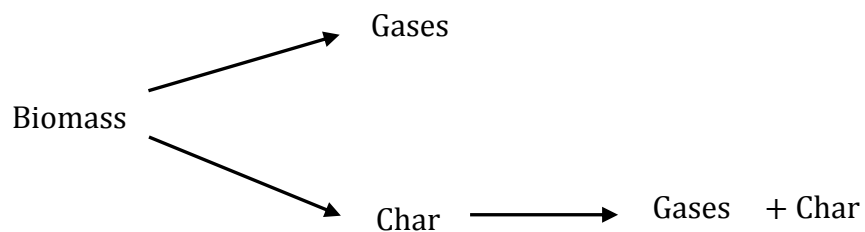
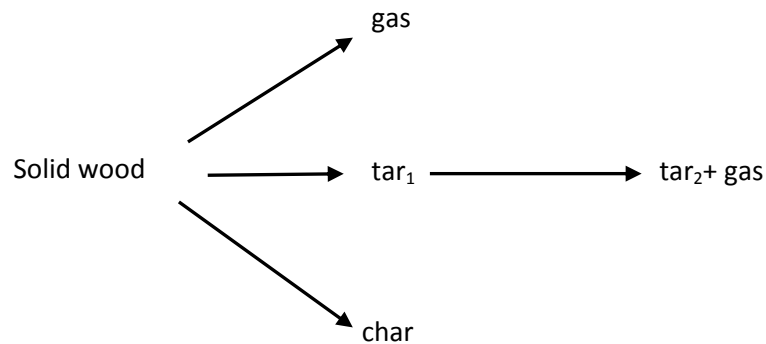


Figure 2.5: Parallel pyrolysis scheme

Parallel pyrolysis scheme is presented in preceding reactions. Biomass is decomposed into char and volatiles through parallel reactions and char and volatiles further react to form secondary gases and char.

Another parallel scheme is presented in following reaction paths. Biomass is decomposed into volatiles, char and tar through parallel reactions and tar gets further decomposed into secondary tar and gases.



University of Moratuwa, Sri Lanka.

Electronic Theses & Dissertations

www.lib.mrt.ac.lk

Figure 2.6: Parallel pyrolysis scheme with tar decomposition

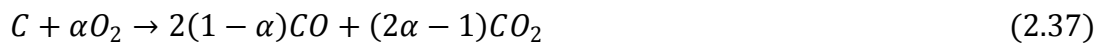
The reaction rate of each component reaction in above schemes is calculated according to an Arrhenius relationship as given by following equation [24].

$$r_i = A_i \rho_{wood} \exp\left(\frac{-E_i}{RT}\right) \quad (2.36)$$

The parameters of this expression differ for each reaction and are stated in literature [10], [33].

2.6 Heterogeneous reactions: Combustion and Gasification

After pyrolysis is complete, the main reactions that contribute to the production of Syngas are gasification and combustion. Because of the height of the biomass packed bed and ignition is done at the bottom, different parts of the packed are in different stages through the process. In the bottom region, where oxygen is abundant, main reaction taking place is combustion. Heat generated in the combustion zone is responsible for pyrolysing the rest of the packed bed. This heat is usually conveyed to the higher layers of the packed bed through thermal radiation. When pyrolysis is complete in the top layers, char formed cannot undergo combustion reactions because oxygen concentration is very low. The char gasifies reacting with carbon dioxide and moisture present in the gas phase. The stoichiometries of combustion and gasification reactions are as follows.



The parameter α is dependent on the fuel temperature and is given by [1], [21],

$$\alpha = \frac{2 + A \exp\left(\frac{-E}{RT_s}\right)}{2 \left(1 + A \exp\left(\frac{-E}{RT_s}\right)\right)} \quad (2.40)$$

The actual reaction rates of these reactions depend on two factors. The kinetic rate and mass transfer rate of the reactant gas into the surface of the porous char. Usually, the reaction rate is limited by the mass transfer process, because mass transfer rates are much slower than the kinetic rates at higher temperatures. The kinetic rates of above reactions can be generally expressed as [9],

$$r_{k,i} = A_c A_j T_s \exp\left(-\frac{E_i}{RT_s}\right) \frac{M_c}{n_{sto} M_j} \rho_j \quad (2.41)$$

Mass transfer rate of a reactant gas to the surface of the char particle can be calculated by [31],

$$r_{m,i} = k_{m,j} A_c \rho_j \quad (2.42)$$

It is assumed here that kinetic rate is larger compared to the mass transfer rate so that reactant gas undergo immediate conversion at the surface of the char particle. Hence its density is equal to zero at the surface of the char particle.

The mass transfer coefficient of j^{th} gas, $k_{m,j}$, is evaluated using following correlation [21].

$$Sh_j = 2 + 0.1Sc^{\frac{1}{3}}Re^{0.6} \quad (2.43)$$

The overall reaction rates of heterogeneous reactions are obtained by evaluating the equivalent parallel resistance of the kinetic and mass transfer rates, this is given by,

$$r_i = \frac{r_{k,i} r_{m,i}}{r_{k,i} + r_{m,i}} \quad (2.44)$$



University of Moratuwa, Sri Lanka.
Electronic Theses & Dissertations
www.lib.mrt.ac.lk

2.7 Homogenous reactions

Following homogenous reactions taking place between gas phase components are considered in this study.



Expressions for kinetic reaction rate, r_k , of these reactions are stated in literature [7] and are listed in Table 2.1.

Table 2.1: Kinetic rate expressions for homogenous reactions

| Reaction | Kinetic rate expression |
|--|---|
| $CO + 0.5O_2 \rightarrow CO_2$ | $2.32 \times 10^{12} \exp\left(-\frac{167}{RT_g}\right) [CO][O_2]^{0.25} [H_2O]^{0.5}$ |
| $H_2 + 0.5O_2 \rightarrow H_2O$ | $1.08 \times 10^{13} \exp\left(-\frac{125}{RT_g}\right) [H_2][O_2]$ |
| $CH_4 + 2O_2 \rightarrow CO_2 + 2H_2O$ | $5.16 \times 10^{13} T_g^{-1} \exp\left(-\frac{130}{RT_g}\right) [CH_4][O_2]$ |
| $CO + H_2O \leftrightarrow H_2 + CO_2$ | $12.6 \exp\left(-\frac{2.78}{RT_g}\right) \left([CO][H_2O] - \frac{[CO_2][H_2]}{0.0265 \exp\left(\frac{3968}{T_g}\right)} \right)$ |



University of Moratuwa, Sri Lanka.
Electronic Theses & Dissertations
www.lib.mrt.ac.lk

The kinetic rate is the rate at which reaction progresses when reactants are abundant. In gas phase reactions of a gasifier, reacting species are brought together by turbulent mixing of gas phase. Because of this effect, kinetic reaction rate is limited by the turbulent mixing rate of the gas species. The turbulent mixing rate is calculated according to the eddy dissipation model, which is given by equation (26) [1].

$$r_{t,i} = 4\rho_g \frac{\varepsilon}{k} \min\left(\frac{Y_j}{v_j M_j}, \frac{Y_k}{v_k M_k}\right) \quad (2.49)$$

Where; j and k represents the reactants of reaction i .

The reaction rate for each gas phase reaction is taken to be equal to the minimum value of kinetic rate and turbulent mixing rate [1].

$$r_i = \min(r_{k,i}, r_{t,i}) \quad (2.50)$$

Chapter 3

MATHEMATICAL MODEL FOR THE PACKED BED

3.1 Computational domain and model description

Biomass pyrolysis process of a packed bed consists of a multiphase system of solid and gas phases. The computational domain of the two phase system is shown in Figure 8.

For modeling of such systems two approaches of mathematical models are used in the literature [11], [15]. These are;

1. Euler-Euler models
2. Euler - Lagrange models

In Euler-Euler models both phases are represented as continuums and gas flow through the packed bed is modeled as a flow through a porous media [1]. This approach is used in many CFD simulations of gasification and its sub processes [5] [8], [11].

In Euler-Lagrange models the motion of individual particles are considered in approaches such as discrete element method and only the gas phase is modeled as a continuum with CFD. The final model is expressed as a sum of individual contributions of each particle and their interaction with surrounding gas phase [15].

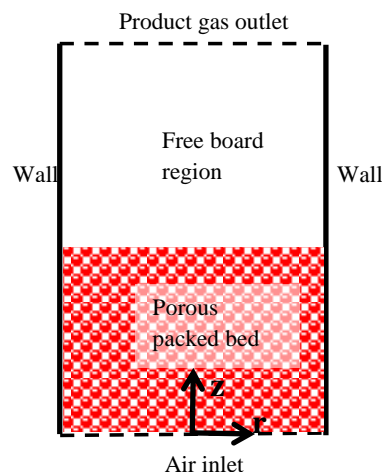


Figure 3.1: Computational domain of gasifier model

Euler-Lagrange models are more accurate in simulating packed beds because they capture the real physics of the system more closely than Euler-Euler models. However they require expensive computing facilities and considerably longer times to simulate.

As a result, the Euler-Euler approach is used by majority of researchers to simulate packed bed processes.

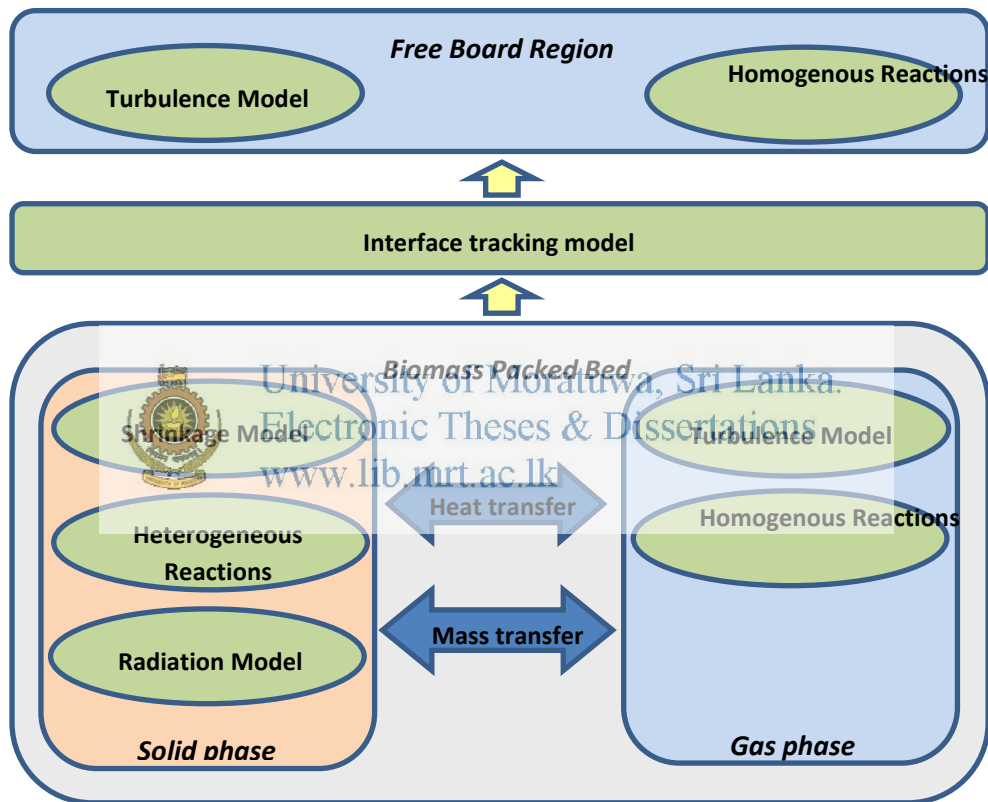


Figure 3.2: Schematic diagram of mathematical model

3.2 Governing transport equations

Conservation equations for momentum, energy and species are solved in the gas phase.

$$\frac{\partial}{\partial t} \rho_g \epsilon_g \mathbf{U}_g + \nabla \cdot (\rho_g \epsilon_g \mathbf{U}_g \otimes \mathbf{U}_g) - \nabla \cdot \mu \epsilon_g \nabla \mathbf{U}_g = -\epsilon_g \nabla p + \nabla \cdot s_{ij} \quad (3.1)$$

$$\begin{aligned} \frac{\partial \rho_g \varepsilon_g C_{v,g} T_g}{\partial t} + \nabla \cdot (\rho_g \varepsilon_g C_{v,g} T_g \mathbf{U}_g) - \nabla \cdot (\varepsilon_g k_g \nabla T_g) \\ = hA(T_s - T_g) + \sum_i \Delta H_i r_{i,homo} + R_{g,pyro} C_{v,g} (T_s - T_g) \end{aligned} \quad (3.2)$$

$$\frac{\partial}{\partial t} (\rho_g \varepsilon_g Y_{i,g}) + \nabla \cdot (\rho_g \varepsilon_g Y_{i,g} \mathbf{U}) - \nabla \cdot (\varepsilon_g D_{i,g} \nabla Y_{i,g}) = \sum_i r_{i,homo} + \sum_i r_{i,hetero} \quad (3.3)$$

Energy conservation and species conservation equations are solved in the solid phase,

$$\begin{aligned} \frac{\partial \rho_s \varepsilon_s C_s T_s}{\partial t} + \nabla \cdot (\rho_s \varepsilon_s C_s T_s \mathbf{U}_s) - \nabla \cdot (\varepsilon_s k_s \nabla T_s) \\ = -hA(T_s - T_g) + \sum_i \Delta H_i r_{i,hetero} + Q_{rad} + Q_{i,c} \end{aligned} \quad (3.4)$$



University of Moratuwa, Sri Lanka.
Electronic Theses & Dissertations
www.lib.mrt.ac.lk

$$\frac{\partial}{\partial t} (\rho_s \varepsilon_s Y_{i,s}) + \nabla \cdot (\rho_s \varepsilon_s Y_{i,s} \mathbf{U}_s) - \nabla \cdot (\varepsilon_s D_{i,s} \nabla Y_{i,s}) = \sum_i r_{i,hetero} \quad (3.5)$$

3.3 Drying model

The low temperature drying model is developed by making an energy balance over the wood particle. It is assumed that heat is transferred to the wood particle by means of convection from surrounding hot air and through radiation. The energy is transferred from the particle as the latent heat of evaporated water. Moisture in wood exists as free and bound water. Free water is liquid water and water vapour that is present in pores and capillaries inside wood. Bound water consists of water

molecules that are attached to the cellulose molecules by hydrogen bonding. When all the free water have been evaporated, water exists in the wood only as bound water. At this point moisture level is said to have reached fiber saturation point [23]. In this study water evaporation is assumed to occur in two stages. Evaporation of water until fiber saturation point and evaporation of water beyond fiber saturation point. For these two stages, two mass transfer coefficients are introduced. The first stage mass transfer coefficient is taken to be dependent on external flow and the second stage coefficient is assumed to be dependent on wood properties. The wood particle and the heat flow are indicated in Figure 10. The energy balance equation is given in Equation 3.6.

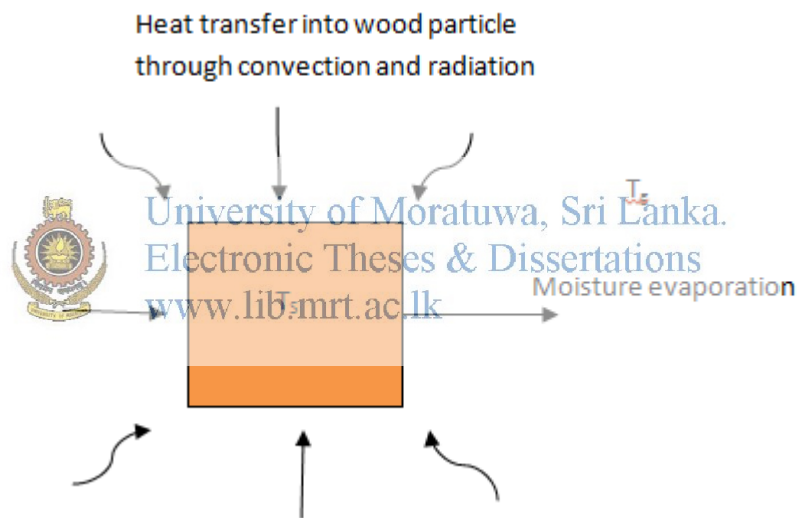


Figure 3.3: Energy transfer modes to wood particle

The energy balance for the wood particle results in

$$hA(T_g - T_s) + \sigma \epsilon A(T_g^4 - T_s^4) = \frac{d}{dt}(mc_s T_s) + \dot{m} A m_d \Delta h_v \quad (3.6)$$

The moisture evaporation flux of the wood particle is generally written by using mass transfer coefficient (k_m) as follows [31],

$$\dot{m} = k_m (x^* - x_g) \quad (3.7)$$

Assumptions are used to evaluate quantities present in Equation 3.7. These assumptions are discussed in detail in the following sections.

3.3.1 Assumptions used for calculating k_m

In the drying process the water which is present in wood in two forms, is removed by two main processes as follows [34].

1. The transport of bound moisture from internal structure to the surface of the solid. The process depends mainly on physical properties of the wood.
2. Evaporation of free water from the surface of the solid. This process depends on external air flow, temperature, humidity and pressure.

Depending on the form of moisture being removed, one or other of the above mentioned processes become the rate limiting process. In this study, the drying model is divided into two cases as follows;

1. When $x > x_{FSP}$ unbound moisture evaporation.
2. When $x < x_{FSP}$ bound moisture evaporation.

Where x is the dry basis moisture content in the wood sample and x_{FSP} is the dry basis moisture content corresponding to fiber saturation point.

A separate value for mass transfer coefficient k_m is used in Equation 2 for each case depending on prevailing process.

When $x > x_{FSP}$, k_m is calculated using Equations 3.8 and 3.9 [31],

$$Sh = (0.35 + 0.34Re^{0.5} + 0.15Re^{0.58})Sc^{0.3} \quad (3.8)$$

$$Sh = \frac{k_m L}{D} \quad (3.9)$$

Where L is the characteristic length and D is the diffusion coefficient of moisture in air.

When $x < x_{FSP}$, it is assumed in this study that, k_m can be written as a function of temperature and wood type. Which is shown in Equation 3.10.

$$k_m = \alpha f(T_s) \quad (3.10)$$

In the present work values for α for three different wood types are found and a suitable approximation to function f is evaluated.

3.3.2 Assumptions used for calculating x^*

When $x > x_{FSP}$

It is assumed that before fiber saturation point is reached the vapour pressure exerted by moisture present in the wood is given by saturation vapour pressure of water at the solid temperature. This assumption is applied in several works [18], [23], [30]. Water saturation pressure with respect to the temperature is shown in Equation 3.11 [30],

$$P_w = \exp\left(25.5058 - \frac{5204.9}{T_s}\right) \quad (3.11)$$

And x^* is calculated using

$$x^* = 0.622 \frac{P_w}{760 - P_w} \quad (3.12)$$

When $x < x_{FSP}$

After the fiber saturation point, the relative humidity is given by a sorption isotherm. x^* is evaluated using equations presented by [30].

$$x^* = 0.622 \frac{P_w}{760 - P_w} \frac{\beta x^3}{x^3 + 0.01} \quad (3.13)$$

The k_m and x^* values calculated as described in sections 3.1 and 3.2 are used in Equation 3.7 to calculate the moisture evaporation flux.

3.4 Pyrolysis model

In the present work, a global reaction scheme for pyrolysis is assumed [8], [11]. This is given in following equation.



It is assumed that the stoichiometric coefficients are dependent on the species of wood. This gives the overall mathematical model the ability to analyze different wood species.

The coefficients are determined using experimental data obtained by proximate analysis and an assumed distribution of volatile gases based on previous literature.

The coefficients for carbon and ash are directly determined by the fraction of free carbon and ash content given by proximate analysis. For gas species, each coefficient is determined by following equation.

$$a_i = \alpha_i VF \quad (3.15)$$

Where, a_i represents a, b, c etc for different values of i. The temperature dependent factor α describes the distribution of gases in the volatile fraction and VF is the volatile fraction of wood species under interest. For present study values for α is calculated using data given in [24].

3.5 Interphase heat transfer

Two main processes are responsible for interphase heat transfer. These are;

1. Convective transfer of heat between two phases as a result of temperature difference between gas and solid phases.
2. During pyrolysis stage, hot volatile gases generated within the porous structure of biomass release into gas phase. These hot volatile gases introduce an energy flow to the gas phase.

Convective heat transfer is modelled by using an overall heat transfer coefficient. The heat transfer rate is evaluated by;

$$Q_{sg} = hA(T_s - T_g). \quad (3.16)$$

During the process of pyrolysis, the solid biomass decomposes into gas products, which is released into the gas phase. It is assumed that these gas products are of the temperature of the solid phase. The release of these higher temperature gases into the gas phase results in an additional energy transfer term in gas phase energy equation given by;

$$R_{g,pyro} C_{v,g}(T_s - T_g) \quad (3.17)$$

Where $R_{g,pyro}$ is the total gas generation rate due to biomass pyrolysis.

3.6 Modelling of bed shrinkage

As heterogeneous reactions of char progresses, the volume of char particles reduces. As a result, top layers of the biomass bed moves downwards. This motion is important to keep the combustion zone stable. When fuel is consumed in combustion zone, new char particles from pyrolysis zone enters to the combustion zone as a result of this bed motion. If particle movement is not there, the combustion zone tends to propagate along the height of the gasifier, reducing the quality of the producer gas. So it is important that the model should be capable of predicting the bed motion.

The effect of bed motion is included into solid species equations as a convective flow term. It is assumed that the bed motion can be represented by a continuous velocity field of the solid phase and this velocity, called shrinkage velocity is applied to all solid species.

Shrinkage velocity is calculated by equating the downward volumetric flow rate of solid phase to total reduction rate of volume caused as a result of heterogeneous reactions of char. The resulting expression is given in following equation.

$$U_s = \frac{1}{\rho_s A_g} \int \left(\sum_i^{R3,R4,R5} r_i \right) dV \quad (3.18)$$

Use of this velocity in the convective terms of solid species equations cause the solid species fields of the gasifier to move downwards at the shrinking rate. This causes the solid phase to move downwards and extend the free board region. But mathematical equations used in free board region and solid phase region are different. Therefore when shrinkage modelling is used there has to be a procedure to track the interface and change the mathematical equations above and below the interface to obtain an accurate solution. The changes of the equations are presented in graphical form in Figure 3.4.

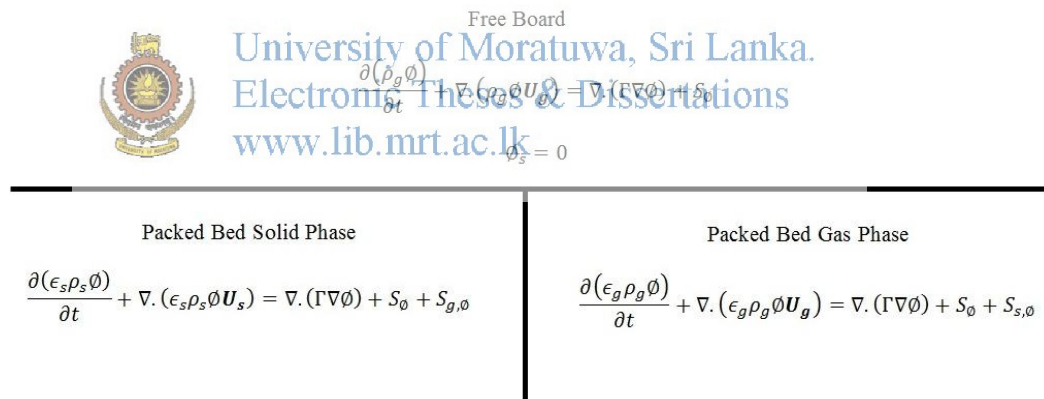
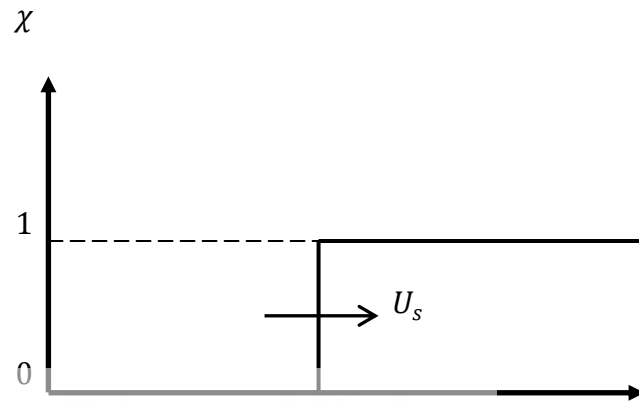


Figure 3.4: Changes of governing equations as a result of bed shrinkage

Gas phase equations differ in two regions with respect to the gas phase porosity, which is defined as the volume fraction of gas phase in each computational cell. The porosity field is initialized in the beginning of the simulation through initial conditions. Gas phase porosity is equal to one in free board region and a variable (<1) in packed bed. The source terms that arise as interactions with solid phase are

not present in free board region. Solid phase equations are different entirely in two regions. In free board, a solid phase does not exist and values of solid phase quantities should be zero. The CFD solver should consider these changes as shrinkage progresses.

This is achieved by multiplying certain terms of the general transport equation by a new field variable, χ , which is a unit step function moving along with shrinkage velocity, as illustrated in Figure 3.5.



University of Moratuwa, Sri Lanka.
Electronic Theses & Dissertations
www.lib.mrt.ac.lk

Figure 3.5: Motion of unit step variable χ in the direction of bed shrinkage

The value of χ is evaluated based on gas phase porosity; it is assumed that a certain point (i.e a computational cell) in the solution domain belongs to free board when gas phase porosity exceeds a certain cut off value. A similar classification of computational cells based on porosity is discussed in [24]. Theoretically, the cut off value should be equal to 1. However during numerical solution process, gas phase porosity does not become exactly equal to one. Hence a value that is closer to one and develops a sharp interface is used. In the present study, 0.95 is assumed as the cut off. Hence χ can be written as,

$$\chi = \begin{cases} 1; & \text{if } \epsilon_g < 0.95 \\ 0; & \text{if } \epsilon_g > 0.95 \end{cases} \quad (3.19)$$

This produces a moving χ field along with the packed bed as expected.

The transport equations for gas and solid phases indicated in Figure 3.4 can be then generalized as,

$$\frac{\partial(\epsilon_s \rho_s \phi)}{\partial t} + \chi \nabla \cdot (\epsilon_s \rho_s \phi \mathbf{U}_s) = \chi \nabla \cdot (\Gamma \nabla \phi) + \chi S_\phi + \chi S_{g,\phi} \quad (3.20)$$

$$\frac{\partial(\epsilon_g \rho_g \phi)}{\partial t} + \nabla \cdot (\epsilon_g \rho_g \phi \mathbf{U}_g) = \nabla \cdot (\Gamma \nabla \phi) + S_\phi + \chi S_{s,\phi} \quad (3.21)$$

Depending on the value of χ the solver will selectively apply equations in packed bed and free board region as shrinkage progresses.

3.7 Turbulence modeling

Turbulence of the gas phase is modeled according to Reynolds Averaged Numerical Simulation (RANS) with standard $k - \epsilon$ model [35]. The main steps of this approach are highlighted in present section.

The main step of the procedure is to express the fluid velocity as the sum of a mean and a fluctuating component [36].

$$u = U + u' \quad (3.22)$$

Where U is the mean velocity and u' is the fluctuating component.

The mean velocity U is defined by,

$$U = \frac{1}{\Delta t} \int_0^{\Delta t} u dt \quad (3.23)$$

The expression for velocity in equation 3.21 is substituted and simplified in ordinary Navier – Stokes equation to give,

$$\frac{\partial}{\partial t} \rho \mathbf{U} + \nabla \cdot (\rho \mathbf{U} \otimes \mathbf{U}) - \mu \nabla \cdot \nabla \mathbf{U} = -\nabla p + \nabla \cdot s_{ij} \quad (3.24)$$

s_{ij} is the Reynolds stress tensor given by [36],

$$s_{ij} = 2\mu_t S_{ij} - \frac{2}{3}\rho k \delta_{ij} \quad (3.25)$$

With,

$$S_{ij} = \frac{\partial U_i}{\partial x_j} + \frac{\partial U_j}{\partial x_i} = \nabla U + (\nabla U)^T \quad (3.26)$$

k is the turbulent kinetic energy per unit mass defined by,

$$k = \frac{1}{2}(\overline{u'^2} + \overline{v'^2} + \overline{w'^2}) \quad (3.27)$$

Where u' , v' and w' represent the x, y and z components of the fluctuating velocity.

The turbulent viscosity μ_t is calculated by,

$$\mu_t = \rho C_\mu \frac{k^2}{\varepsilon} \quad (3.28)$$

Where ε is the dissipation rate of turbulent kinetic energy, k .

In order to make a mathematically closed system of equations, two additional equations to determine k and ε are needed. In standard $k - \varepsilon$ model, following transport equations are used to calculate k and ε [36].

$$\frac{\partial(\rho k)}{\partial t} + \nabla \cdot (\rho k U) = \nabla \cdot \left(\frac{\mu_t}{\sigma_\varepsilon} \nabla k \right) + 2\mu_t S_{ij} : S_{ij} - \rho \varepsilon \quad (3.29)$$

$$\frac{\partial(\rho \varepsilon)}{\partial t} + \nabla \cdot (\rho \varepsilon U) = \nabla \cdot \left(\frac{\mu_t}{\sigma_\varepsilon} \nabla \varepsilon \right) + C_{1\varepsilon} \frac{k}{\varepsilon} 2\mu_t S_{ij} : S_{ij} - C_{2\varepsilon} \rho \frac{\varepsilon^2}{k} \quad (3.30)$$

The following values for constants are used in the standard $k - \varepsilon$ model.

$$C_\mu = 0.09, \sigma_k = 1, \sigma_\varepsilon = 1.3, C_{1\varepsilon} = 1.44, C_{2\varepsilon} = 1.92$$

The above set of equations are solved to obtain the mean velocity field U and pressure field p .

Scalar fields are treated in a similar way. First, the field is separated into fluctuating and a mean component.

$$\varphi = \bar{\varphi} + \varphi' \quad (3.31)$$

By substituting this expression and the expression for velocity into transport equation for a scalar quantity results in the following transport equation for the scalar field.

$$\frac{\partial(\rho\bar{\varphi})}{\partial t} + \nabla \cdot (\rho\bar{\varphi}U) = \nabla \cdot (\Gamma_{\bar{\varphi}}\nabla\bar{\varphi}) + \nabla \cdot (\Gamma_t\nabla\bar{\varphi}) \quad (3.32)$$

Γ_t is the turbulent or eddy diffusivity. It is calculated by using the turbulent Prandtl number as follows,

$$\sigma_t = \frac{\mu_t}{\Gamma_t} \quad (3.33)$$

Experimental analysis of turbulent flows has shown that this ratio is constant. In many CFD calculations the ratio is taken to be around unity [36].



University of Moratuwa, Sri Lanka.
Electronic Theses & Dissertations

3.8 Radiation model www.lib.mrt.ac.lk

Radiation heat transfer plays a major role in transporting heat generated in combustion zone from combustion reactions, to top wood layers of the packed bed. This heat provides the energy for thermal cracking of biomass and other endothermic solid phase reactions that take place in top layers. In the present work, P1 radiation model is applied to model radiation in the packed bed with following assumptions[7] [37].

- Biomass bed can be treated as an absorbing, emitting, scattering medium of dispersed solid particles.
- Combustion zone can be approximated by a hot emissive plate located at the bottom of the gasifier.
- The gas phase is optically thin and does not interact with radiation.

A schematic diagram of the radiation model is shown in Figure 3.6.

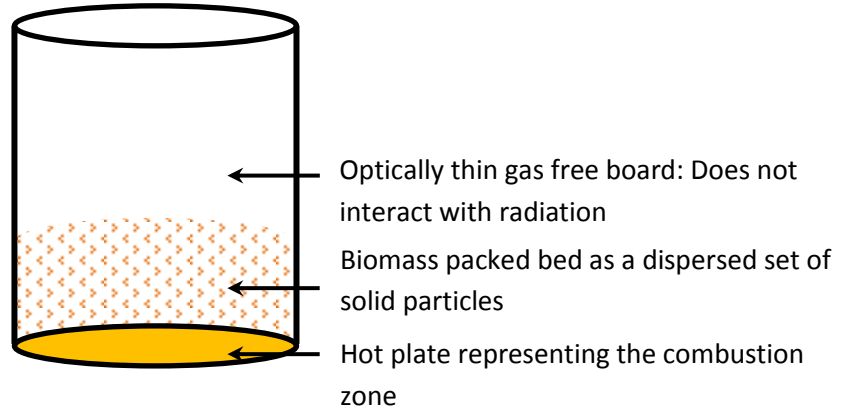


Figure 3.6: Schematic of Radiation model

The governing transport equation of P1 model for incident intensity, G , with a dispersed solid phase can be written as [37];

$$\nabla \cdot (\Gamma \nabla G) + 4(an^2\sigma T_g^4 + E_p) - (a + a_p)G = 0 \quad (3.34)$$

Where Γ is given by,

$$\Gamma = \frac{1}{3(a + a_p + \sigma_p)} \quad (3.35)$$

The equivalent emission of particles, E_p , is calculated by;

$$E_p = \epsilon A_r T_s^4 \quad (3.36)$$

With the simplifying assumptions of an optically thin gas phase ($a, n = 0$), equation (3.33) can be reduced to,

$$\nabla \cdot (\Gamma \nabla G) + 4E_p - a_p G = 0 \quad (3.37)$$

Where,

$$\Gamma = \frac{1}{3(a_p + \sigma_p)} \quad (3.38)$$

The radiation heat flux in P1 model is given by [7]

$$q_r = -\Gamma \nabla G \quad (3.39)$$

The radiation source term in energy equation is given by $-\nabla q_r$, which is obtained by applying gradient operator to equation (3.38) and simplifying with the use of equation (3.36).

$$-\nabla q_r = \alpha_p G - 4E_p \quad (3.40)$$

This term is substituted in the solid phase energy equation as the source term for thermal radiation.



University of Moratuwa, Sri Lanka.
Electronic Theses & Dissertations
www.lib.mrt.ac.lk

3.9 Physical properties

The thermal conductivity of gas phase is calculated by [11]

$$k_g = 4.8 \times 10^{-4} T_g^{0.717} \quad (3.41)$$

The thermal conductivity of biomass packed bed is evaluated using a correlation developed for thermal conductivity of a quiescent bed corrected for the effect of gas flow, as proposed in Jurena [21]. This correlation is presented in equation (3.41).

$$k_s = 0.8k_g + 0.5Re.Pr.k_g \quad (3.42)$$

Biomass particle diameter is used as the characteristic length in evaluating the Reynolds number.

Individual heat capacities of solid and gas species are not considered. An overall temperature dependent heat capacity for each phase is assumed. Heat capacity of solid and gas phases are assumed to vary according to the relations given in equations (3.42) and (3.43). These correlations are taken from Jurena [21].

$$C_s = 420 + 2.09T_s + 6.85 \times 10^4 T_s^{-2} \quad (3.43)$$

$$C_g = 990 + 0.122T_g - 5680 \times 10^3 T_g^{-2} \quad (3.44)$$

The porosity of bed is considered to be varying as Pyrolysis progresses. Porosity is expressed as a function of mass fractions of raw biomass, char and ash as indicated in equations (3.44) and (3.45)

$$\epsilon_s = \frac{m_{Wood}}{\rho_{wood}} + \frac{m_{Char}}{\rho_{char}} + \frac{m_{Ash}}{\rho_{ash}} \quad (3.45)$$

$$\epsilon_g = 1 - \epsilon_s \quad (3.46)$$

m_{Wood} , m_{Char} and m_{Ash} represent the mass of wood, char and Ash present in a unit volume.  University of Moratuwa, Sri Lanka
Electronic Theses & Dissertations
www.lib.mrt.ac.lk

Heat transfer coefficient h between solid and gas phase is evaluated using [31],

$$Nu = (0.35 + 0.34Re^{0.5} + 0.15Re^{0.58})Pr^{0.3} \quad (3.47)$$

The specific surface area of a biomass particle is calculated by equation (3.47) taken from Jurena [21],

$$A_p = \frac{\epsilon_s d}{6} \quad (3.48)$$

Where, d is the diameter of biomass particle.

Diffusion coefficients are evaluated using equation (3.48) [28]. These are calculated as binary diffusion coefficients based on diffusion of a specific component in air.

$$D_{i,air} = 0.0018583 \sqrt{T_g^3 \left(\frac{1}{M_i} + \frac{1}{M_{air}} \right)} \frac{1}{p \sigma_{i,air}^2 \Omega_{i,air}} \quad (3.49)$$

Where, M-molar mass, p – pressure, σ – average collision diameter, Ω - diffusion collision integral.

Pyrolysis rate is evaluated using an Arrhenius reaction rate expression given by equation (3.49) [10].

$$r = \rho_s Y_{wood} \cdot A \exp\left(\frac{-E_p}{RT_s}\right) \quad (3.50)$$



University of Moratuwa, Sri Lanka.
Electronic Theses & Dissertations
www.lib.mrt.ac.lk

Chapter 4

NUMERICAL SOLUTION FOR THE PACKED BED MODEL

4.1 Introduction to OpenFOAM

OpenFOAM is an open source Computational Fluid Dynamics package which can be used to generate numerical solutions to mathematical models using finite volume method. Two main steps are involved in generating a numerical solution in OpenFOAM. These are: setting up the case and setting up the solver. Case set up is the pre processing stage in an OpenFOAM calculation. An OpenFOAM case is a collection of folders in which separate files are defined which contain the information on initial stage of the system and instructions on solving fluid dynamics equations. An example of a case file structure is illustrated in Figure 4.1.

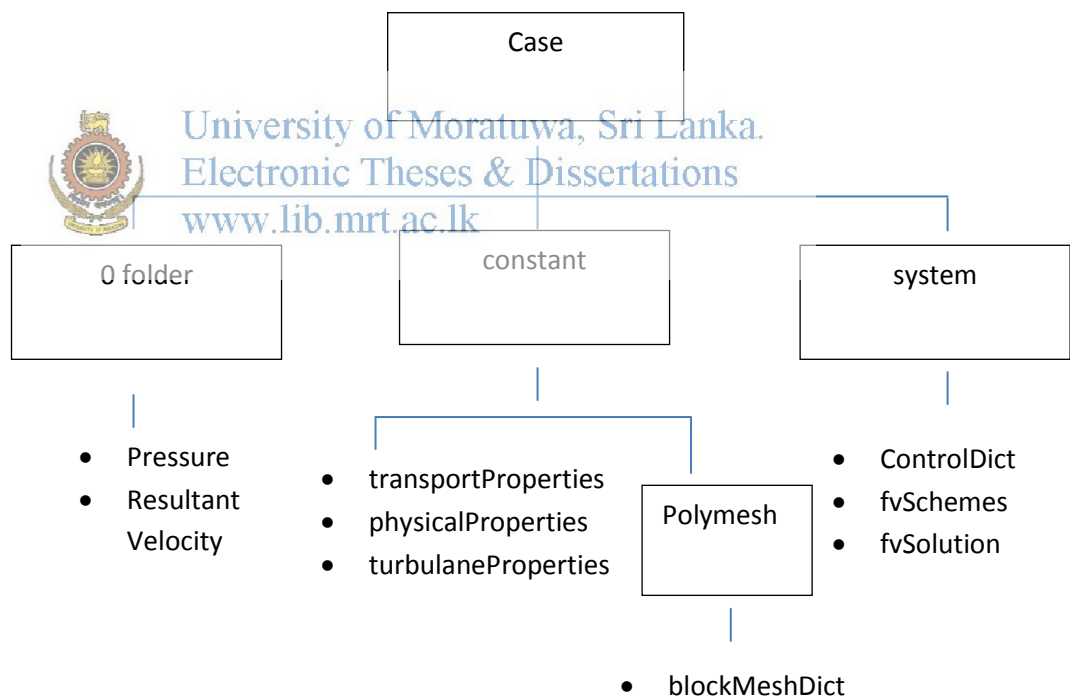


Figure 4.1: Structure of an OpenFOAM case

The 0 folder consists of a set of files for each field for which solution is obtained (eg pressure and velocity). These files contain information on initial and boundary fields of these variables. Constant folder consists of a sub directory called polymesh where a blockMeshDict file is located. This file consists of information for mesh generation. Other files that are located in constant directory include transportProperties, physicalProperties and turbulenceProperties, which include information on values of physical constants (viscosity, thermal conductivity etc) and information on turbulence. Systems directory consist of files: ControlDict, fvSchemes and fvSolution. ControlDict file contains information on time control of the case, such as start time, end time, time step for numerical calculations and other information. fvSchemes consists of a list of discretization schemes for each variable. User can change discretization settings for the case by changing entries of this file. The fvSolution contains information about linear solvers that are used to solve discretized equations and tolerances for solved variables.

4.2 OpenFOAM solver

In OpenFOAM, a solver is a C++ library, which contains the code to numerically solve the relevant differential equations of the system under interest. Solvers can be classified as built in solvers and user compiled solvers. Built in solvers come with the original installation of OpenFOAM and can be used for solution of wide range of standard problems such as incompressible flow calculations, multiphase flows etc. When a built in solver cannot be applied to develop a solution to a particular problem, the user has the freedom to compile a new solver for the application. The OpenFOAM programming style allows user to declare and use mathematical quantities such as, scalars, vectors, tensors, their fields and differential equations. The differential equations are discretized using finite volume method. A brief introduction to finite volume discretization is presented in the following section.

4.3 Introduction to finite volume method

In numerical mathematics, partial differential equations are solved by first converting them to a corresponding set of algebraic equations. This is done by a method called discretization. There are a number of discretization techniques available, which

include, finite volume method, finite element method, finite difference method, Spectral element method, Boundary element method and High-resolution discretization schemes.

In the present study, the equations are discretized using finite volume method, using the built in libraries of the CFD tool OpenFOAM. Finite volume discretization process can be divided into three main steps [38],

- Discretization of time
- Discretization of space
- Discretization of Equations

4.3.1 Discretization of time

Time is discretized by separating the time domain over which the solution is required in to a set of time steps Δt , which may change during the simulation. During the solution procedure, time is marched from a prescribed initial condition.

4.3.2 Discretization of space

Discretization of space is achieved by sub dividing the solution geometry in to a number of cells called control volumes. These cells should not overlap with one another and should fill the computational domain. The centroids of these cells determine the points of space at which the solution is required. A typical control volume and its associated properties are presented in Figure 4.2.

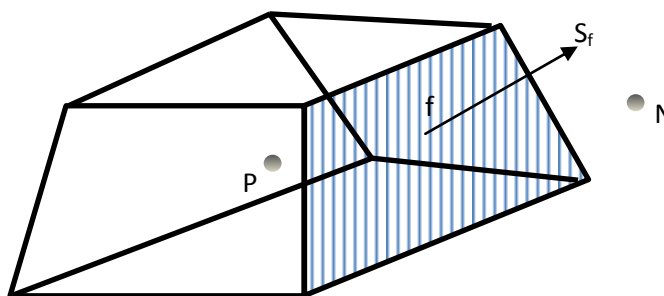


Figure 4.2: A typical control volume in finite volume method

The control volume is bounded by flat faces, represented by letter f . Cell faces belong to two main categories, internal faces and boundary faces. Internal faces are the faces between two control volumes and boundary faces coincide with boundaries of the solution domain. Each face of internal cells is shared with only one neighbor cell. Properties are usually defined at cell centroids, P . The face area vector, S_f is of magnitude equal to the area of the face and points outwards from the control volume perpendicular to the face [38].

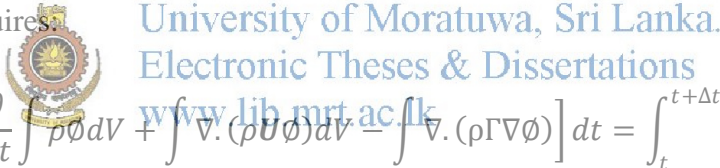
4.3.3 Discretization of equations

The general form of the conservation equation for a scalar property ϕ can be written as,

$$\frac{\partial(\rho\phi)}{\partial t} + \nabla \cdot (\rho\mathbf{U}\phi) - \nabla \cdot (\rho\Gamma\nabla\phi) = S_\phi \quad (4.1)$$

The finite volume method requires that this equation should be satisfied in integral form over the control volume around the point at which the solution is sought [38].

This requires:



$$\int_t^{t+\Delta t} \left[\frac{\partial}{\partial t} \int_V \rho\phi dV + \int_V \nabla \cdot (\rho\mathbf{U}\phi) dV - \int_V \nabla \cdot (\rho\Gamma\nabla\phi) dV \right] dt = \int_t^{t+\Delta t} \left(\int S_\phi dV \right) dt \quad (4.2)$$

4.3.4 Spatial discretization

The first spatial term of Equation 4.2 is discretized as,

$$\int \rho\phi dV = \rho\phi_P V_P \quad (4.3)$$

The volume integrals of the above equation are converted into surface integrals over control volume surface using the following identities of vector calculus [39];

$$\int \nabla \cdot \mathbf{A} dV = \int \mathbf{A} \cdot d\mathbf{S} \quad (4.4)$$

$$\int \nabla \phi dV = \int \phi d\mathbf{S} \quad (4.5)$$

This results in following relationships for convective and diffusive terms of the general conservation equation,

$$\int \nabla \cdot (\rho \mathbf{U} \phi) dV = \int (\rho \mathbf{U} \phi) \cdot d\mathbf{S} \quad (4.6)$$

Because the control volume is bounded by a series of flat faces, the surface integral on the right hand side can be written as a sum of integrals over separate faces, this results in,

$$\int (\rho \mathbf{U} \phi) \cdot d\mathbf{S} = \sum_f \int (\rho \mathbf{U} \phi) \cdot d\mathbf{S}_f \quad (4.7)$$

The face integral is evaluated using face value of ϕ and $\rho \mathbf{U}$

$$\int (\rho \mathbf{U} \phi) \cdot d\mathbf{S} = (\rho \mathbf{U})_f \cdot \mathbf{S}_f \phi_f \quad (4.8)$$

This provides the discretized form of the convective term as,

$$\int \nabla \cdot (\rho \mathbf{U} \phi) dV = \sum_f (\rho \mathbf{U})_f \cdot \mathbf{S}_f \phi_f \quad (4.9)$$

Using the above procedure, the laplacian term is discretized as,

$$\begin{aligned}\int \nabla \cdot (\rho \Gamma \nabla \phi) &= \int (\rho \Gamma \nabla \phi) \cdot dS \\ &= \sum_f \int (\rho \Gamma \nabla \phi) \cdot dS \\ &= \sum_f \rho \Gamma (\nabla \phi)_f \cdot S_f\end{aligned}$$

Therefore,

$$\int \nabla \cdot (\rho \Gamma \nabla \phi) = \sum_f \rho \Gamma (\nabla \phi)_f \cdot S_f \quad (4.10)$$

The discretized form of integral terms can be evaluated using face values and face center values of neighbor cells. The entire set of discretized equations written over the solution domain represents a system of simultaneous linear equations. This linear set of equations is solved during each iteration of solution algorithm using numerical procedures for linear systems.



Electronic Theses & Dissertations
www.lib.mrt.ac.lk

4.4 Developed CFD solver using OpenFOAM

A new solver, *movingbedGasificationFoam*, was developed based on the equations presented in chapter 3. The structure of the solver is illustrated in Figure 17. The equations are numerically solved using finite volume method. Required code was developed by using C++ language in OpenFOAM package, including all the relevant differential equations and procedures in the CFD model using built in tools of OpenFOAM [40], [41]. The solution domain is assumed to be two dimensional and consists of radial and axial dimensions only. This is because the reactor is axisymmetric in geometry, initial and boundary fields and as a result the solution is effectively two dimensional. The computational domain of CFD model is presented in Figure 4.3. Discretization schemes used to discretize convective and divergence terms are listed in Table 4.1. A schematic of solution algorithm is presented in Figure 4.4.

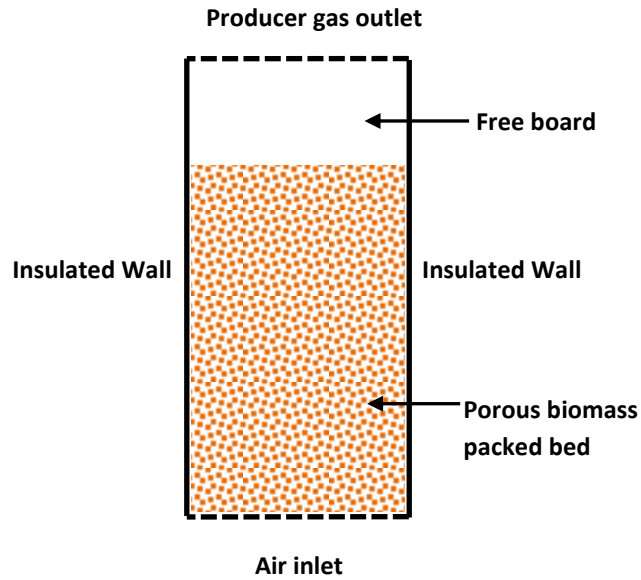


Figure 4.3: Computational domain of the CFD solution

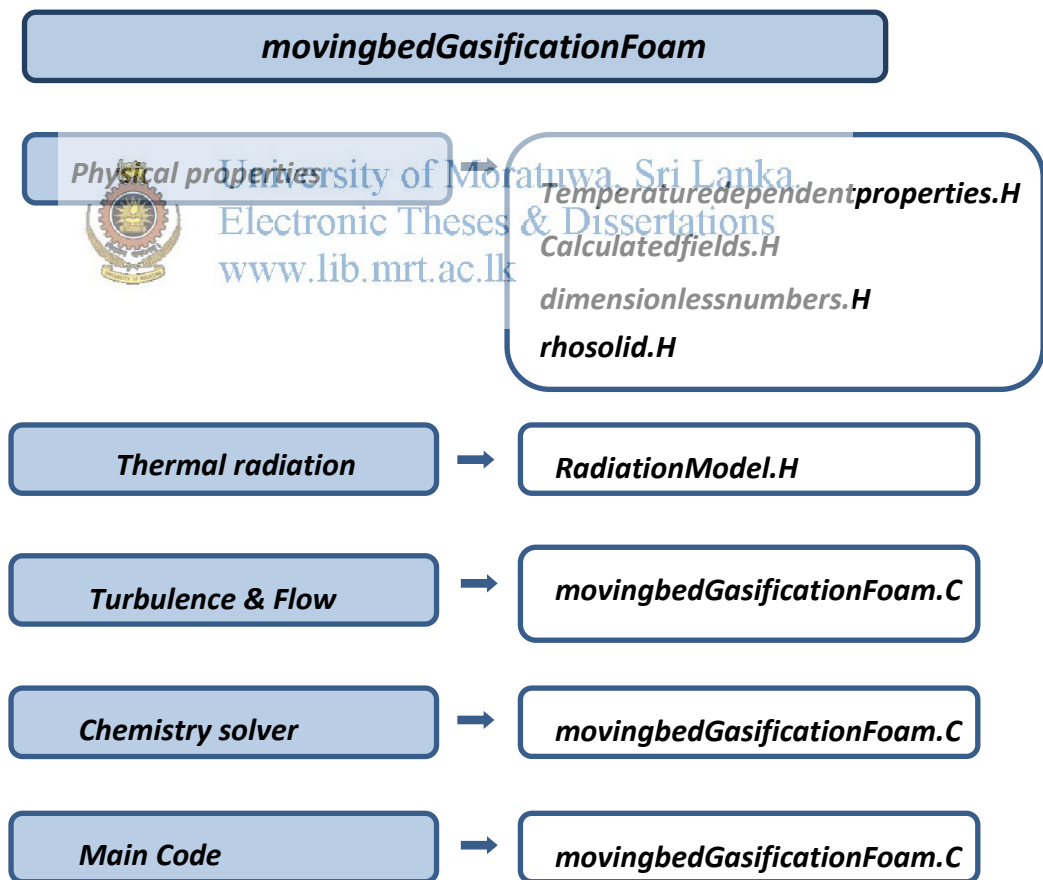


Figure 4.4: File structure of developed OpenFOAM solver

4.4.1 Initial and Boundary conditions

It is assumed that the gasification process is carried out in a cylindrical reactor using air at room temperature as the gasifying medium. This air stream is supplied at constant flow rate from bottom of the reactor. To model the initial ignition process, a distributed heat source similar to magnitude of heat generated by a combustion reaction is applied over a bed region of 0.2 m above the grate and removed after model is capable of continuing operation by own heat emitted by its combustion reactions. The initial heat source is responsible for pyrolysing a small region of packed to generate char necessary to initiate combustion reactions. This start up method was chosen as it closely resembles the real world operation of a gasifier. The required time for initial ignition was found by trial and error by simulating the system. Then initially five minutes time was applied and increasing it gradually until simulation is successfully progressed.

The initial velocity field within the reactor is taken as zero. Pressure is set to atmospheric pressure. The initial temperatures of gas and solid phases are taken as 300 K. Initial compositions of product gases are taken as zero and the inlet gas composition is taken to be equal to that of air at room temperature and atmospheric pressure. Boundary conditions for velocity, pressure, temperature and species mole fractions are indicated in following equations.

Inlet boundary conditions

$$U = U_{in} \quad (4.11)$$

$$P = P_{in} \quad (4.12)$$

$$T_g = T_{g,in} \quad (4.13)$$

$$\frac{\partial T_s}{\partial z} = 0 \quad (4.14)$$

$$Y_i = Y_{i,air} \quad (4.15)$$

Wall boundary conditions

$$U = \frac{\partial P}{\partial r} = \frac{\partial T_g}{\partial r} = \frac{\partial T_s}{\partial r} = \frac{\partial Y_i}{\partial r} = 0 \quad (4.16)$$

Outlet boundary conditions

$$\frac{\partial U}{\partial z} = \frac{\partial P}{\partial z} = \frac{\partial T_g}{\partial z} = \frac{\partial T_s}{\partial z} = \frac{\partial Y_i}{\partial z} = 0 \quad (4.17)$$

Table 4.1: Discretization Schemes

| Term | Discretization scheme |
|--|-----------------------|
| $\nabla \cdot (\rho_g \epsilon_g \mathbf{U}_g \otimes \mathbf{U}_g)$ | Upwind |
| $\nabla \cdot \rho_g \epsilon_g C_{v,g} T_g \mathbf{U}_g$ | Upwind |
| $\nabla \cdot \rho_s \epsilon_s C_s T_s \mathbf{U}_s$ | Upwind |
| $\nabla \cdot (\rho_g \epsilon_g Y_i \mathbf{U}_g)$ | Upwind |
| $\nabla \cdot (\rho_s \epsilon_s Y_i \mathbf{U}_s)$ | MUSCL |



University of Moratuwa, Sri Lanka.
Electronic Theses & Dissertations
www.lib.mru.ac.lk

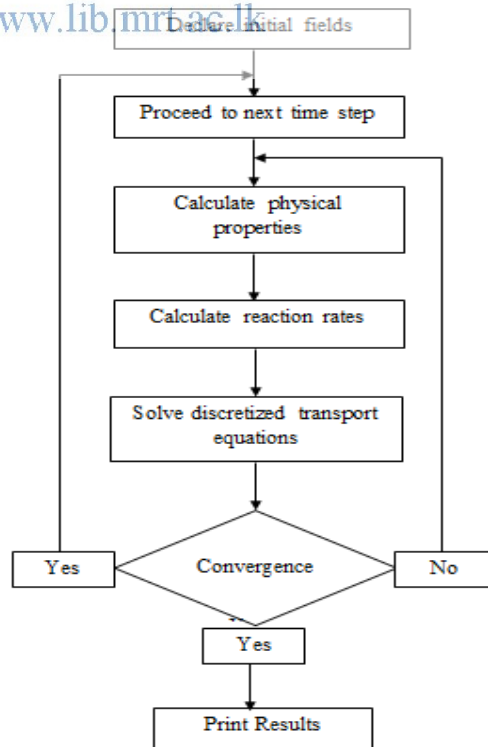


Figure 4.5: Solution Algorithm

4.4.2 Computational mesh

The dimensions of computational domain were 1.2 m in axial (y) direction and 0.3 m in radial (x) direction. Computational mesh consisted of cells with $\Delta x = 0.012$ m and $\Delta y = 0.024$ m. The time step used for calculations was 0.05 seconds. The computational mesh used for simulations are shown in Figure 4.6.

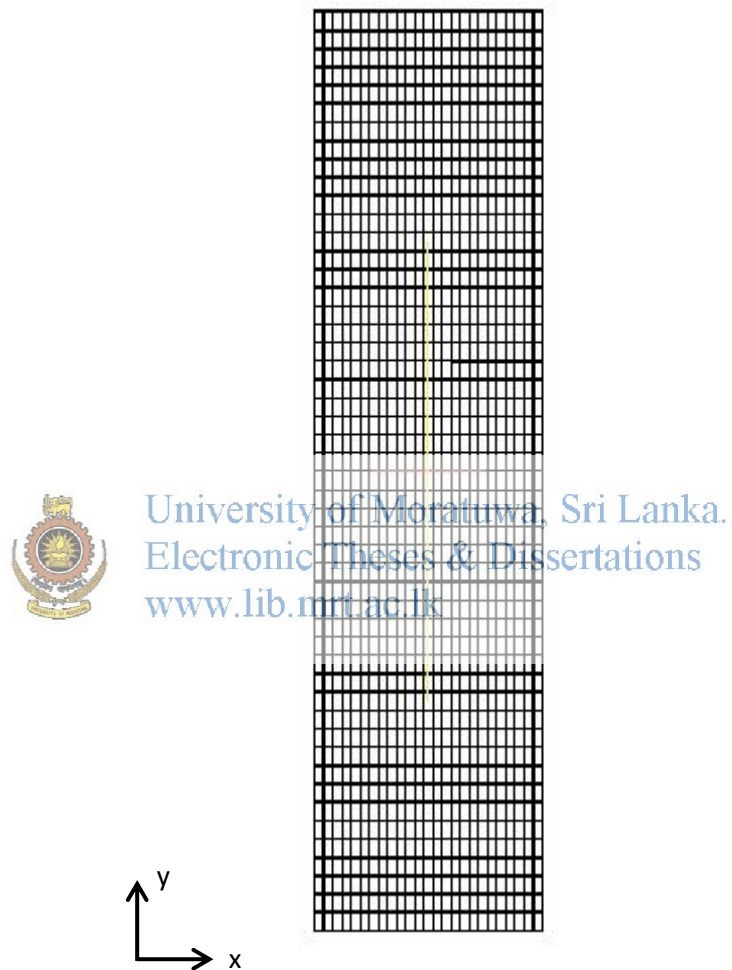


Figure 4.6: Computational mesh

Chapter 5

EXPERIMENTAL SET UP AND MODEL VALIDATION

5.1 Model validation

The CFD model presented in previous chapter is validated by comparing the simulation results with data obtained from a laboratory scale updraft gasifier. The gasifier consists of a vertical cylinder with a grate at the bottom. Biomass is fed from the top of the gasifier through a lid, which is closed after loading one batch of biomass. The loaded batch is ignited at the bottom of the gasifier. Air at room temperature is supplied through the grate by using an air blower. In this experimental facility, four thermocouples, which are recorded the temperature along the centre line, were installed along the height of the gasifier. A schematic diagram of the experimental facility is shown in Figure 5.1. Simulation results were compared against experimental data for gasification of *Gliricidia* under an airflow rate of 6 m³/hr. The physical and chemical properties of fuel are listed in Table 5.1. The comparison of temperature profiles obtained from simulations with experimentally measured temperature values are presented in Figure 5.3. Exit gas temperatures predicted by simulation and experimental exit gas temperatures are displayed in Figure 5.4. Theoretical and experimental outlet gas compositions are presented in Figure 5.5. Data analysis is performed using post processing tool Paraview.

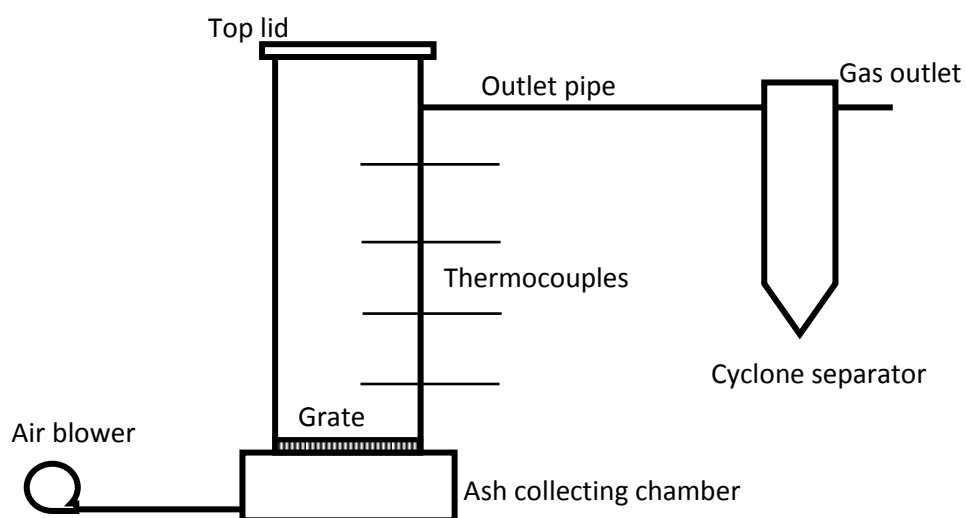


Figure 5.1: Schematic diagram of experimental gasification system

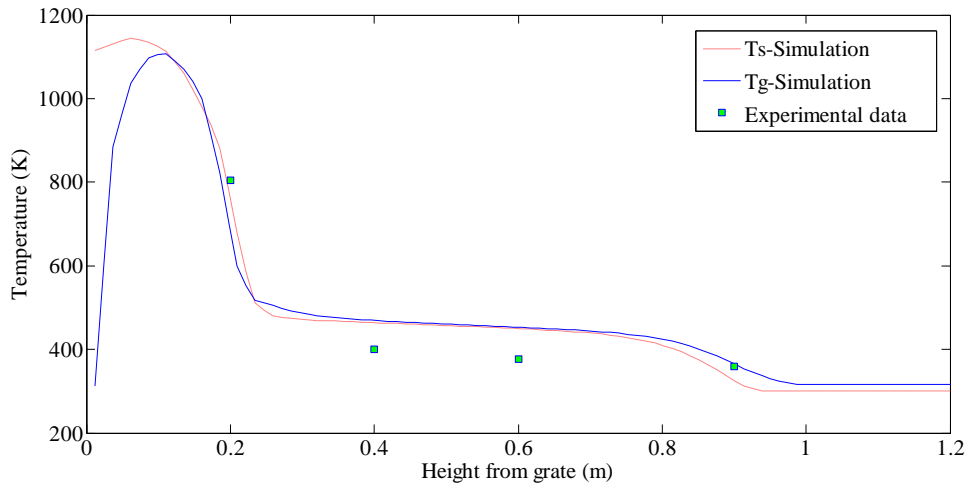


University of Moratuwa, Sri Lanka.
Electronic Theses & Dissertations
www.lib.mrt.ac.lk

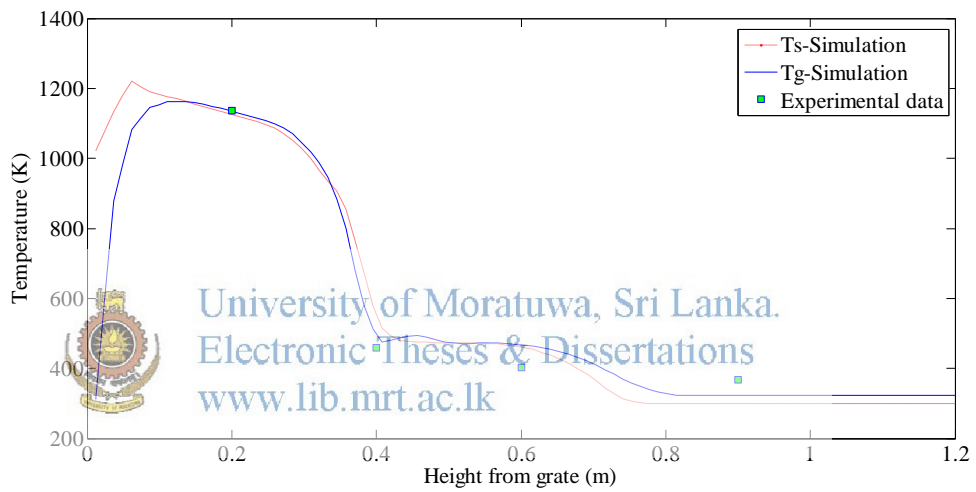
Figure 5.2: Experimental laboratory scale gasification system

Table 5.1: Physical and chemical properties of fuel

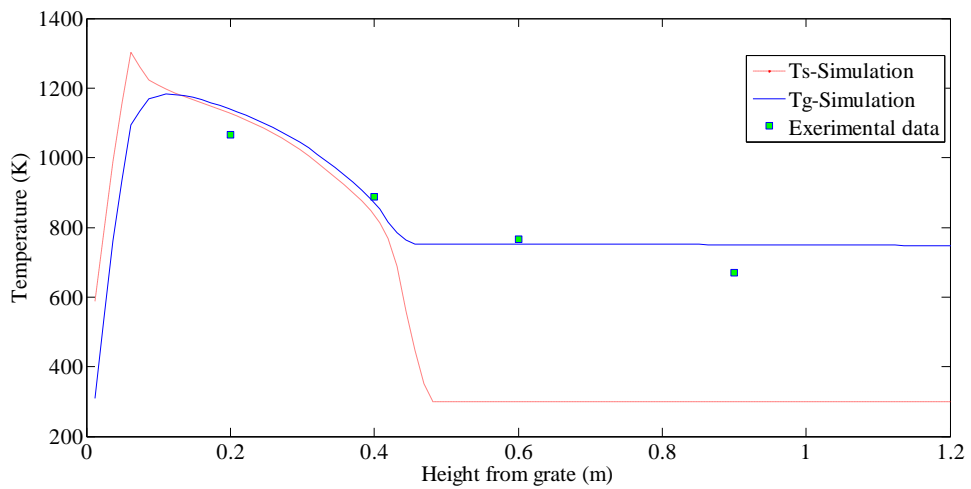
| | |
|--------------------------------------|-------------------|
| Species | <i>Gliricidia</i> |
| Particle size | 20 mm |
| Particle shape | Cubic |
| Batch weight | 28 kg |
| Free carbon (dry basis) | 17.8 % |
| Volatiles (dry basis) | 82.16 % |
| Ash (dry basis) | 0.04 % |
| Initial moisture content (dry basis) | 0.18 |



(a)



(b)



(c)

Figure 5.3: Theoretical and experimental temperature profiles; (a) 45 minutes after ignition (b) 75 minutes after ignition (c) 150 minutes after ignition

In Figure 5.3 (c), which presents the temperature profiles after 2.5 hours of initial ignition, the biomass bed has reduced as a result of fuel consumption due to heterogeneous reactions. The thermocouples located at 60 cm and 90 cm positions do not encounter any solid phase. Their readings comply with gas phase temperatures at the points, as evident from the figure. The results indicate that temperature in the combustion zone rises to a value about 1300 K, with a peak value resulting in few centimetres above the grate. A similar behaviour of temperature variation can be observed in experimental work of Wei Chen at el [12] for updraft gasification of mesquite and juniper wood. Their results indicate a combustion zone temperature of nearly 1300 K. The following figure compares the experimental and theoretical exit gas temperatures of the gasifier.

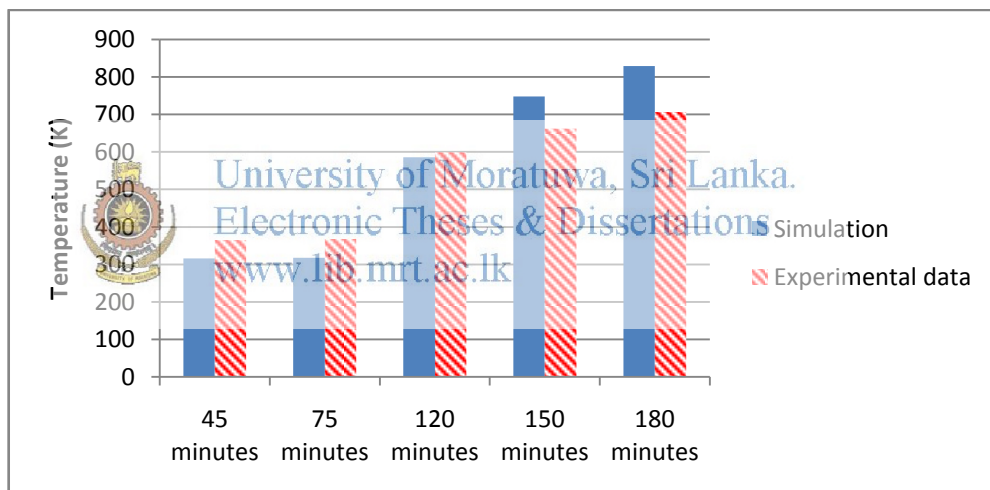


Figure 5.4: Theoretical and Experimental exit gas temperatures

It can be observed that at higher temperatures, the difference between experimental value and theoretical prediction is higher. The CFD model predicts a higher outlet gas temperature than the observed value. This is because the radiation losses from the gas phase through walls and the top lid of the gasifier are not accounted in the model. And the radiation losses become higher at higher temperatures.

During the simulations, it is found that composition of produced gas varies with time, during initial period, raw biomass is present in the bed and moisture levels are

higher. This introduces moisture into gas phase. Pyrolysis in top layers is not complete and as a result low amount of char is available on the top layers to react with carbon dioxide produced in the combustion zone. The initial gas is therefore higher in carbon dioxide and moisture levels. Experimental and simulation results for gas composition after one hour of initial ignition are presented in Figure 5.5.

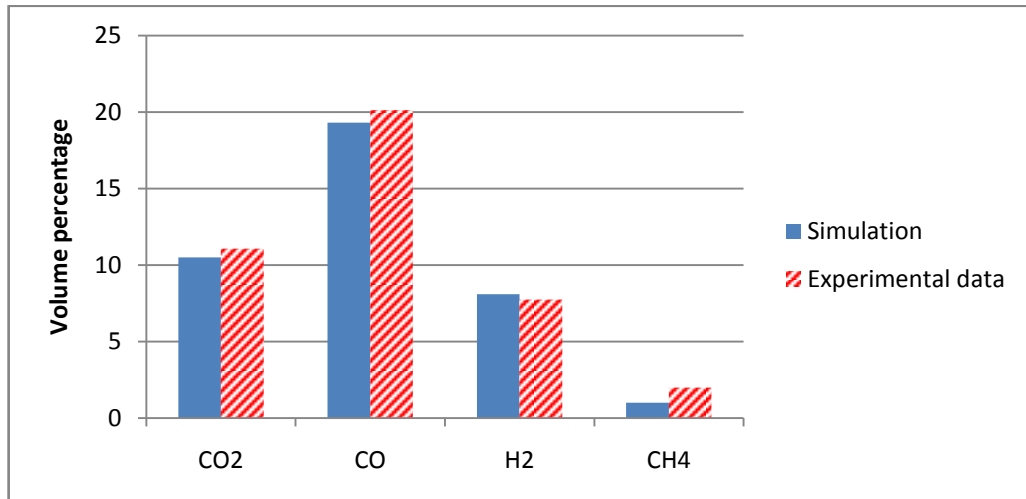


Figure 5.5: Theoretical and Experimental gas compositions after 60 minutes of ignition.

The values for gas compositions are also comparable with experimental observations of C.Mandl et al [8]. Their experimental data for a fixed bed updraft gasifier operated with softwood pellets indicate a final CO volume percentage of 22.6%, a CO₂ percentage of 4.8%, H₂ percentage of 4.3 % and a CH₄ percentage of 2.7 %.

Experimentally it is found that during the process of gasification, packed bed can be separated into four zones; drying, pyrolysis, reduction and combustion, depending on the main processes taking place in these zones. It is possible to identify the development of these zones in the present CFD model by observing the carbon dioxide mass fraction along the height of the gasifier. This is presented in Figure 5.6.

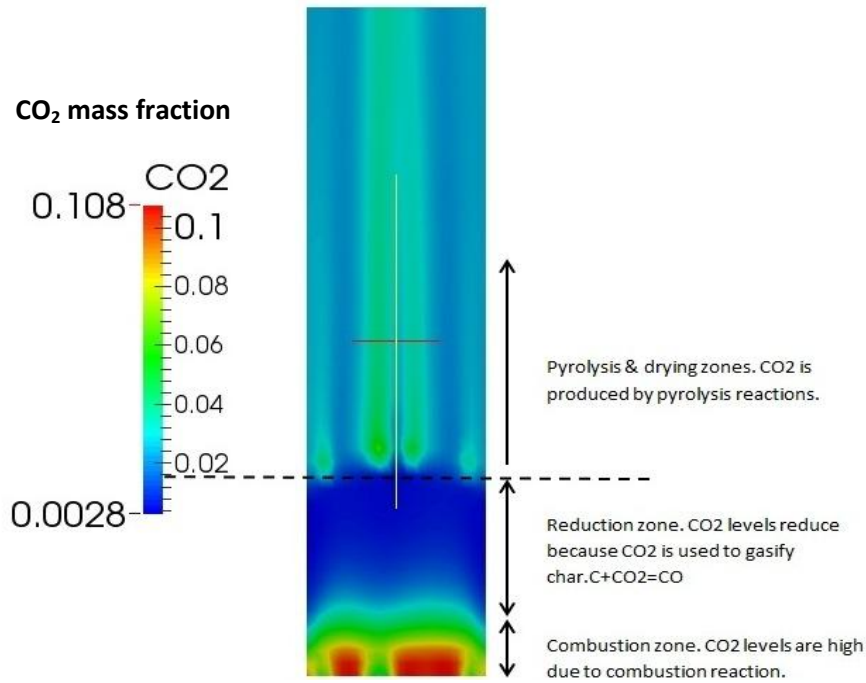


Figure 5.6: Development of reaction zones in the solution domain

During a batch process the quality of the produced gas varies with the time, mainly as a result of downward motion of the fuel bed. During experiments it is observed that a stable flame cannot be maintained approximately after four hours of operation. The following figures present the variation of outlet gas volume fractions and packed bed locations. The packed bed location is identified by viewing the solid phase temperature profiles.

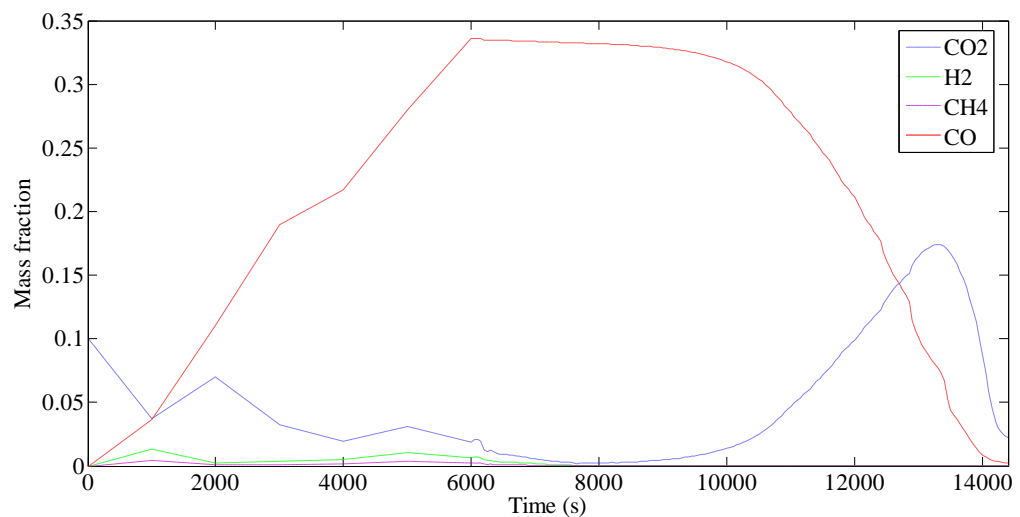


Figure 5.7: Variation of gas phase component volume fractions with time

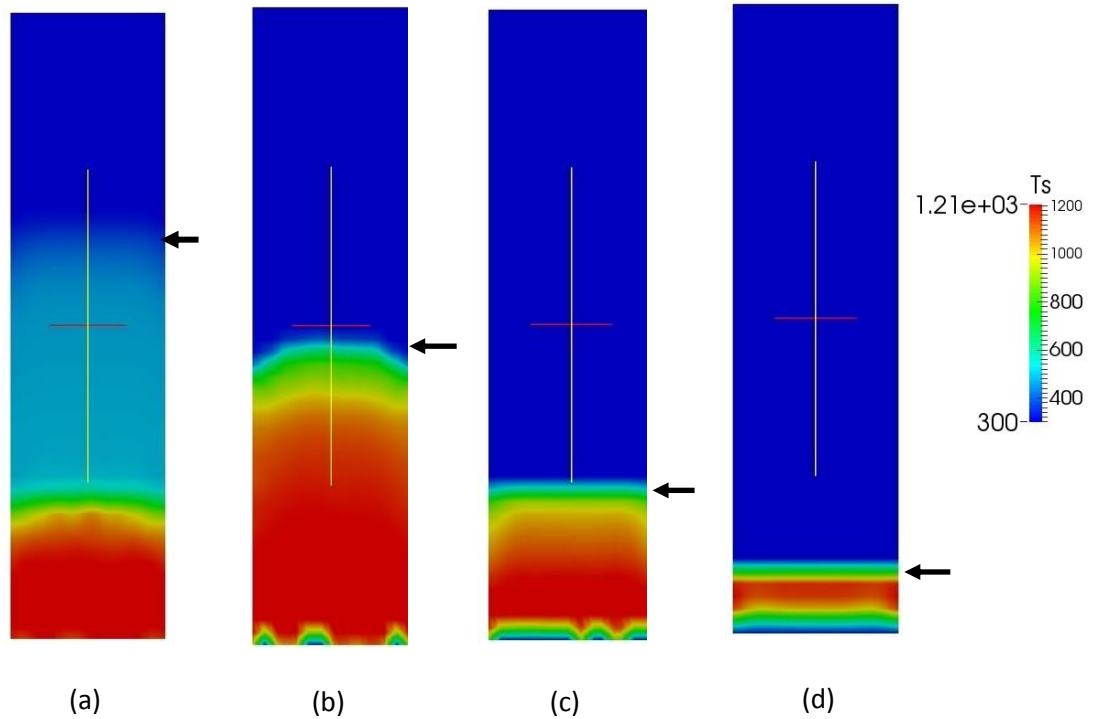


Figure 5.8: Bed reduction with time; (a) 1 hour after ignition (b) 2 hours after ignition (c) 3 hours after ignition (d) 4 hours after ignition. Location of interface between packed bed and free board is marked with the black arrow

University of Moratuwa, Sri Lanka.
 Electronic Theses & Dissertations
 www.lib.mrt.ac.lk

A contour plot of temperature of biomass after two hours from ignition is presented in Figure 5.9

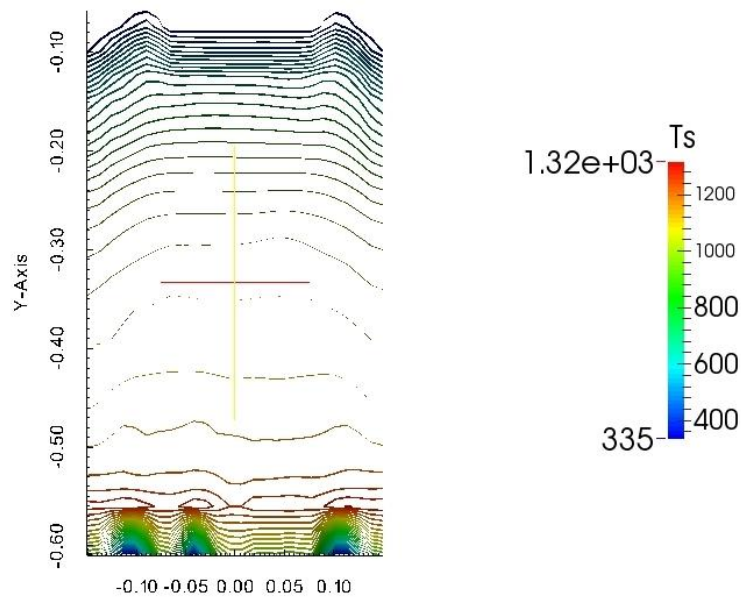
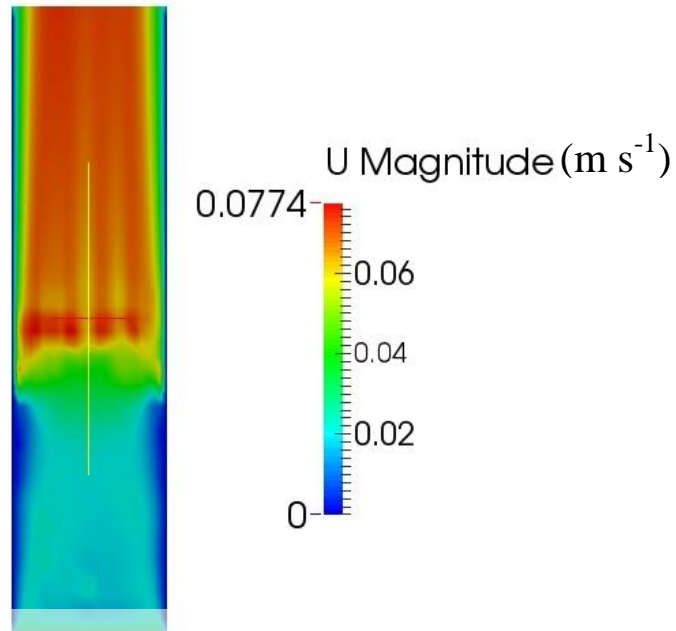


Figure 5.9: Temperature contours with in biomass bed after two hours from ignition.

The velocity distribution of gas phase is presented in Figure 5.10. It can be noted that due to release of pyrolysis gases, velocity in pyrolysis zone is higher compared to other areas of the bed.



University of Moratuwa, Sri Lanka.
Electronic Theses & Dissertations
www.lib.mrt.ac.lk

Figure 5.10: Gas phase velocity distribution

5.2 Optimization of air flow rate to the Gasifer based on CFD model

The external air flow to the gasifier supply fuel needed to maintain combustion process. When air flow rate is higher, the extent of the combustion zone increases, causing the produced fuel gases to burn inside the reactor. This reduces the quality of the outlet gas. When flow rates are too small, combustion rates reduce and sufficient heat is not produced for complete cracking of biomass in top layers of the bed. The developed CFD model is used to evaluate optimal air flow rate for maximum cumulative carbon monoxide production.

A series of simulations were performed for air flow rates ranging from $4 \text{ m}^3/\text{hr}$ to $10 \text{ m}^3/\text{hr}$. The results are summarized in Table 5.2.

Table 5.2: Simulation Results for different air flow rates

| Flow rate (m ³ /hr) | Batch time (s) | Peak CO composition | Cumulative CO (m ³) |
|-----------------------------------|----------------|------------------------|------------------------------------|
| 4 | 21600 | 0.39 | 5.3 |
| 5 | 15800 | 0.4 | 5.52 |
| 6 | 14400 | 0.406 | 6.13 |
| 7 | 12800 | 0.415 | 6.4 |
| 8 | 11300 | 0.405 | 5.7 |
| 9 | 10800 | 0.405 | 5.58 |
| 10 | 9200 | 0.4 | 5.375 |

Based on the cumulative CO production, it can be stated that, for the particular experimental gasifier, a flow rate of 7 m³/hr maximizes the CO yield from biomass batch.



University of Moratuwa, Sri Lanka.
Electronic Theses & Dissertations
www.lib.mrt.ac.lk

5.3. Conclusion and future work

A mathematical model for gasification of biomass in a batch wise updraft packed bed reactor was developed and simulated using open source CFD software OpenFOAM. The developed model in this study accounts for drying, pyrolysis, reduction, and combustion reactions. All three modes of heat transfer; conduction, convection and radiation, was included in the packed bed model. It is found by the simulation study; radiation is the main mode of heat transfer through the biomass packed bed and critically important. Reduction of bed volume due to heterogeneous reactions are also considered and modelled in the simulations. The simulation results are in good agreement with experimental data and also with general experimental observations on packed bed gasification processes. The developed model evaluates optimal air flow rate to be $7\text{m}^3/\text{hr}$ for maximum cumulative CO production. In future, the presented mathematical model can be used as a numerical tool to optimize batch wise moving bed gasification processes. The model consists of many runtime variable input parameters such as particle size, inlet air flow rate, inlet-gas compositions, and physical & chemical properties of feed-stock. The model can be used to perform parameter studies to find the optimal values of these parameters for a similar gasifier. Among limitations, the model does not take into consideration tar forming reactions in pyrolysis stage, and only able to predict gasification characteristics of fuels whose shape is of simple geometry. It cannot be applied to cases where biomass fuel has complex geometries, such as hay. The model cannot be used to analyse channelling phenomena, hence it cannot be used to evaluate performance for fuels that have tendency to form channelling effects, such as rice husk gasification. In future, the presented model can be improved by implementing an advanced pyrolysis scheme which contains both primary and secondary pyrolysis reactions separately.

REFERENCES

- [1] Y. Wu, Q. Zhang, W. Yang, and W. Blasiak, "Two-Dimensional Computational Fluid Dynamics Simulation of Biomass Gasification in a Downdraft Fixed-Bed Gasifier with Highly Preheated Air and Steam," *Energy Fuels*, vol. 27, no. 6, pp. 3274–3282, 2013.
- [2] K. Umeki, T. Namioka, and K. Yoshikawa, "Analysis of an updraft biomass gasifier with high temperature steam using a numerical model," *Appl. Energy*, vol. 90, no. 1, pp. 38–45, Feb. 2012.
- [3] Niranjan Fernando, Muhammad Amin, Mahinsasa Narayana, Thamali Jayawickrama, Asadumllah, and Sanath Jayasena, "A mathematical model for Pyrolysis of biomass," *Moratuwa Eng. Res. Conf. MERCon IEEE Conf. Publ.*, pp. 6–11, 2015.
- [4] P. McKendry, "Energy production from biomass (part 2): conversion technologies," *Bioresour. Technol.*, vol. 83, no. 1, pp. 47–54, May 2002.
- [5] E. G. Pereira, J. N. da Silva, J. L. de Oliveira, and C. S. Machado, "Sustainable energy: A review of gasification technologies," *Renew. Sustain. Energy Rev.*, vol. 16, no. 7, pp. 4753–4762, Sep. 2012.
- [6] P. McKendry, "Energy production from biomass (part 3): gasification technologies," *Bioresour. Technol.*, vol. 83, no. 1, pp. 55–63, May 2002.
- [7] Hui Liu, "CFD Modeling of Biomass Gasification Using a Circulating Fluidized Bed Reactor," University of Waterloo, Ontario, Canada, 2014.

- [8] C. Mandl, I. Obernberger, and F. Biedermann, “Modelling of an updraft fixed-bed gasifier operated with softwood pellets,” *Fuel*, vol. 89, no. 12, pp. 3795–3806, Dec. 2010.
- [9] Y. Haseli, J. A. van Oijen, and L. P. H. de Goeij, “A detailed one-dimensional model of combustion of a woody biomass particle,” *Bioresour. Technol.*, vol. 102, no. 20, pp. 9772–9782, Oct. 2011.
- [10] S. Sinha, A. Jhalani, M. R. Ravi, and A. Ray, “Modelling of pyrolysis in wood: A review,” *SESI J.*, vol. 10, no. 1, pp. 41–62, 2000.
- [11] M. A. Masmoudi, M. Sahraoui, N. Grioui, and K. Halouani, “2-D Modeling of thermo-kinetics coupled with heat and mass transfer in the reduction zone of a fixed bed downdraft biomass gasifier,” *Renew. Energy*, vol. 66, pp. 288–298, Jun. 2014.
- [12] W. Chen, K. Annamalai, R. J. Ansley, and M. Mirik, “Updraft fixed bed gasification of mesquite and juniper wood samples,” *Energy*, vol. 41, no. 1, pp. 454–461, May 2012.
- [13] H. Sefidari, N. Razmjoo, and M. Strand, “An experimental study of combustion and emissions of two types of woody biomass in a 12-MW reciprocating-grate boiler,” *Fuel*, vol. 135, pp. 120–129, Nov. 2014.
- [14] F. Guo, Y. Dong, L. Dong, and C. Guo, “Effect of design and operating parameters on the gasification process of biomass in a downdraft fixed bed: An experimental study,” *Int. J. Hydrog. Energy*, vol. 39, no. 11, pp. 5625–5633, Apr. 2014.



University of Moratuwa, Sri Lanka.
 Electronic Theses & Dissertations
www.lib.mrt.ac.lk

- [15] A. H. Mahmoudi, F. Hoffmann, and B. Peters, "Application of XDEM as a novel approach to predict drying of a packed bed," *Int. J. Therm. Sci.*, vol. 75, pp. 65–75, Jan. 2014.
- [16] D. F. Fletcher, B. S. Haynes, F. C. Christo, and S. D. Joseph, "A CFD based combustion model of an entrained flow biomass gasifier," *Appl. Math. Model.*, vol. 24, no. 3, pp. 165–182, Mar. 2000.
- [17] G. Cau, V. Tola, and A. Pettinau, "A steady state model for predicting performance of small-scale up-draft coal gasifiers," *Fuel*, vol. 152, pp. 3–12, Jul. 2015.
- [18] I. W. Turner, "A two-dimensional orthotropic model for simulating wood drying processes," *Appl. Math. Model.*, vol. 20, no. 1, pp. 60–81, Jan. 1996.
- [19] K. D. Patel, N. K. Shah, and R. N. Patel, "CFD Analysis of Spatial Distribution of Various Parameters in Downdraft Gasifier," *Procedia Eng.*, vol. 51, pp. 764–769, 2013.
- [20] S. Murgia, M. Vascellari, and G. Cau, "Comprehensive CFD model of an air-blown coal-fired updraft gasifier," *Fuel*, vol. 101, pp. 129–138, Nov. 2012.
- [21] Tomas Jurena, "Numerical modelling of grate combustion," Brno University of Technology, Brno, 2012.
- [22] Y. Haseli, J. A. van Oijen, and L. P. H. de Goey, "Reduced model for combustion of a small biomass particle at high operating temperatures," *Bioresour. Technol.*, vol. 131, pp. 397–404, Mar. 2013.

- [23] C. Di Blasi, “Multi-phase moisture transfer in the high-temperature drying of wood particles,” *Chem. Eng. Sci.*, vol. 53, no. 2, pp. 353–366, Jan. 1998.
- [24] P. J. Ż. Kamil Kwiatkowski, “Biomass gasification solver based on OpenFOAM,” 2013.
- [25] G. Hu, G. Li, Y. Zheng, Z. Zhang, and Y. Xu, “Euler–Lagrange modeling of wood chip gasification in a small-scale gasifier,” *J. Energy Inst.*, vol. 88, no. 3, pp. 314–322, Aug. 2015.
- [26] A. H. Mahmoudi, M. Markovic, B. Peters, and G. Brem, “An experimental and numerical study of wood combustion in a fixed bed using Euler–Lagrange approach (XDEM),” *Fuel*, vol. 150, pp. 573–582, Jun. 2015.
- [27] T. K. Patra and P. N. Sheth, “Biomass gasification models for downdraft gasifier: A state-of-the-art review,” *Renew. Sustain. Energy Rev.*, vol. 50, pp. 583–593, Oct. 2015.
- [28] R. B. Bird, W. E. Stewart, and E. N. Lightfoot, *Transport Phenomena*, 2 edition. New York: Wiley, 2001.
- [29] M. Nelkon and P. Parker, *Advanced Level Physics*, 7th edition. London: Heinemann International Literature & Textbooks, 1995.
- [30] M. R. Assari, H. Basirat Tabrizi, and M. Saffar-Avval, “Numerical simulation of fluid bed drying based on two-fluid model and experimental validation,” *Appl. Therm. Eng.*, vol. 27, no. 2–3, pp. 422–429, Feb. 2007.
- [31] Treybal, Robert E. *Mass-Transfer Operations*, 3rd Edition, McGraw-Hill Book Company, 1980.

- [32] C. Di Blasi, “Modeling chemical and physical processes of wood and biomass pyrolysis,” *Prog. Energy Combust. Sci.*, vol. 34, no. 1, pp. 47–90, Feb. 2008.
- [33] B. V. Babu and A. S. Chaurasia, “Heat transfer and kinetics in the pyrolysis of shrinking biomass particle,” *Chem. Eng. Sci.*, vol. 59, no. 10, pp. 1999–2012, May 2004.
- [34] A. S. Mujumdar, *Handbook of Industrial Drying, Fourth Edition*, 4 edition. Boca Raton: CRC Press, 2014.
- [35] C. D. Argyropoulos and N. C. Markatos, “Recent advances on the numerical modelling of turbulent flows,” *Appl. Math. Model.*, vol. 39, no. 2, pp. 693–732, Jan. 2015.
- [36] H. Versteeg and W. Malalasekera, *An Introduction to Computational Fluid Dynamics: The Finite Volume Method*, 2 edition. Harlow, England ; New York: Prentice Hall, 2007.
- [37] *Ansys Fluent Theory Guide*. ANSYS Inc: Canonsburg, PA, 2011.
- [38] Hrvoje Jasak, “Error Analysis and Estimation for the Finite Volume Method with Applications to Fluid Flows,” Imperial College of Science, Technology and Medicine, 1996.
- [39] H. K. Dass, *Advanced Engineering Mathematics*. New Delhi: S Chand & Co Ltd, 2007.
- [40] *OpenFOAM Programmer’s Guide*. OpenFOAM Foundation, 2014.
- [41] *OpenFOAM User’s Guide*. OpenFOAM Foundation, 2014.

APPENDIX

OpenFOAM CASE SETTINGS

Intial and boundary condition files for solved variables

CH₄

```
/*-----*- C++ -*-----
-----*\
| ===== |
| |
| \\ / Field | OpenFOAM: The Open Source CFD
Toolbox |
| \\ / Operation | Version: 2.3.0
| |
| \\ / And | Web: www.OpenFOAM.org
| |
| \\ / Manipulation |
| |
\*-----*
-----*/
FoamFile
{
    version 2.0;
    format ascii;
    class volScalarField;
    object CH4;
}
// *****
// *****

dimensions [0 0 0 0 0 0 0];

internalField uniform 0;

boundaryField
{
    wall
    {
        type zeroGradient;
    }

    Outlet
    {
        type zeroGradient;
    }

    Inlet
    {
        type fixedValue;
    }
}
```



```

        value            0;
    }

    "front.*"
    {
        type              empty;
    }

    "back.*"
    {
        type              empty;
    }
}
//
*****
***** //

```

CO

```

/*-----*- C++ -*-----
-----*\
|=====|
|
| \\      F i e l d      | OpenFOAM: The Open Source CFD
Toolbox  | \\      O p e r a t i o n      | Version: 2.0.0
| \\      A n d      | Web:      www.OpenFOAM.org
| \\      M a n i p u l a t i o n      |
|
\*-----*/
-----*/
FoamFile
{
    version      2.0;
    format      ascii;
    class      volScalarField;
    object      CO;
}
// * * * * *
* * * * * //

dimensions      [0 0 0 0 0 0 0];

internalField    uniform 0;

boundaryField
{
    wall

```

```

    {
        type            zeroGradient;
    }

    Outlet
    {
        type            zeroGradient;
    }

    Inlet
    {
        type            fixedValue;
        value           0;
    }

    "front.*"
    {
        type            empty;
    }

    "back.*"
    {
        type            empty;
    }
}
//
***** University of Moratuwa, Sri Lanka. *****
***** // Electronic Theses & Dissertations *****
***** www.lib.mrt.ac.lk *****

```



University of Moratuwa, Sri Lanka.
 Electronic Theses & Dissertations
www.lib.mrt.ac.lk

H₂

```

/*-----*- C++ -*-----
-----*\
| ===== |
| |
| \\ / F i e l d | OpenFOAM: The Open Source CFD
Toolbox |
| \\ / O p e r a t i o n | Version: 2.3.0
| |
| \\ / A n d | Web: www.OpenFOAM.org
| |
| \\ / M a n i p u l a t i o n |
|
\*-----*
-----*/
FoamFile
{
    version      2.0;
    format       ascii;
    class        volScalarField;
    object       H2;
}

```

```

}
// *****
***** //

dimensions      [0 0 0 0 0 0 0];

internalField   uniform 0;

boundaryField
{
    wall
    {
        type          zeroGradient;
    }

    Outlet
    {
        type          zeroGradient;
    }

    Inlet
    {
        type          fixedValue;
        value         0;
    }

    "front.*"
    {
        type          empty;
    }

    "back.*"
    {
        type          empty;
    }
}
//
*****
***** //

```



University of Moratuwa, Sri Lanka.
 Electronic Theses & Dissertations
www.lib.mrt.ac.lk

CO₂

```
/*-----*- C++ -*-----
-----*\
| ===== |
| |
| \\      / F i e l d | OpenFOAM: The Open Source CFD
Toolbox |
| \\      / O p e r a t i o n | Version: 2.3.0
| |
| \\      / A n d | Web: www.OpenFOAM.org
| |
| \\/      M a n i p u l a t i o n |
|
|*-----*
-----*/
FoamFile
{
    version      2.0;
    format       ascii;
    class        volScalarField;
    object       CO2;
}
// * * * * *
* * * * * //

dimensions      [0 0 0 0 0 0 0];
internalField   uniform 0.1;

boundaryField
{
    wall
    {
        type      zeroGradient;
    }

    Outlet
    {
        type      zeroGradient;
    }

    Inlet
    {
        type      fixedValue;
        value     0.1;
    }

    "front.*"
    {
        type      empty;
    }
}
```



University of Moratuwa, Sri Lanka.
Electronic Theses & Dissertations
www.lib.mrt.ac.lk

```

    "back.*"
    {
        type            empty;
    }
}
//
*****
***** //

```

H₂O

```

/*-----*- C++ -*-----
-----*\
| ===== |
| \\      / F i e l d      | OpenFOAM: The Open Source CFD
Toolbox    |
| \\      / O p e r a t i o n | Version:  2.3.0
| \\      / A n d            | Web:      www.OpenFOAM.org
|  \\/      M a n i p u l a t i o n |
|
\*-----
-----*/
FoamFile
{
    version      2.0;
    format       ascii;
    class        volScalarField;
    object       H2O;
}
// * * * * *
* * * * * //

```

```

dimensions      [0 0 0 0 0 0 0];

```

```

internalField   uniform 0;

```

```

boundaryField

```

```

{
    wall
    {
        type            zeroGradient;
    }

    Outlet
    {
        type            zeroGradient;
    }
}

```

```

Inlet
{
    type          fixedValue;
    value         0;
}

"front.*"
{
    type          empty;
}

"back.*"
{
    type          empty;
}
}
//
*****
***** //

```

O₂

```

/*-----*- C++ -*-----
-----*\
| ===== |
| \\      | | Field | OpenFOAM: The Open Source CFD
Toolbox | \\      | | Operation | Version: 2.3.0
| \\      | |      | | Web:      | www.OpenFOAM.org
| \\ /    | A nd   | |
|  \\/    | M anipulation |
|
\*-----
-----*/

```

```

FoamFile
{
    version      2.0;
    format       ascii;
    class        volScalarField;
    object       O2;
}
// * * * * *
// * * * * * //

```

```

dimensions      [0 0 0 0 0 0 0];

internalField   uniform 0.232;

boundaryField
{

```

```

wall
{
    type          zeroGradient;
}

Outlet
{
    type          zeroGradient;
}

Inlet
{
    type          fixedValue;
    value         0.232;
}

"front.*"
{
    type          empty;
}

"back.*"
{
    type          empty;
}
}
//
*****
*****//

```



University of Moratuwa, Sri Lanka.
 Electronic Theses & Dissertations
www.lib.mrt.ac.lk

N₂

```

/*-----*- C++ -*-----
-----*\
| ===== |
| | \ \ / F i e l d | OpenFOAM: The Open Source CFD
Toolbox | |
| \ \ / O p e r a t i o n | Version: 2.3.0
| | \ \ / A n d | Web: www.OpenFOAM.org
| | \ \ / M a n i p u l a t i o n |
| |
\*-----*-
-----*/

FoamFile
{
    version      2.0;
    format       ascii;
    class        volScalarField;
    object       N2;
}

```

```

}
// *****
***** //

dimensions      [0 0 0 0 0 0 0];

internalField   uniform 0.7547;

boundaryField
{
    wall
    {
        type          zeroGradient;
    }

    Outlet
    {
        type          zeroGradient;
    }

    Inlet
    {
        type          fixedValue;
        value         0.7547;
    }

    "front.*"
    {
        type          empty;
    }

    "back.*"
    {
        type          empty;
    }
}
//
*****
***** //

```



University of Moratuwa, Sri Lanka.
 Electronic Theses & Dissertations
www.lib.mrt.ac.lk

Velocity

```

/*-----*- C++ -*-----
-----*\
| ===== |
| |
| \\      / F i e l d | OpenFOAM: The Open Source CFD
Toolbox |
| \\      / O p e r a t i o n | Version: 2.3.0
| |
| \\      / A n d | Web: www.OpenFOAM.org
| |
| \\/      M a n i p u l a t i o n |
|
\*-----*-
-----*/
FoamFile
{
    version      2.0;
    format       ascii;
    class        volVectorField;
    object       U;
}
// *****
// ***** //

dimensions      [0 1 -1 0 0 0 0];
internalField   uniform (0 0 0);

boundaryField
{
    wall
    {
        type      fixedValue;
        value      (0 0 0);
    }

    Outlet
    {
        type      inletOutlet;
        inletValue (0 0 0);
    }

    Inlet
    {
        type      fixedValue;
        value      (0 0.028 0);
    }

    "front.*"
    {

```



University of Moratuwa, Sri Lanka.
 Electronic Theses & Dissertations
www.lib.mrt.ac.lk

```
        type          empty;
    }

    "back.*"
    {
        type          empty;
    }
}

//
*****
***** //
```



University of Moratuwa, Sri Lanka.
Electronic Theses & Dissertations
www.lib.mrt.ac.lk

Solution control file: Control Dict dictionary

```
/*-----*- C++ -*-----
-----*\
| ===== |
| |
| \\      /  F i e l d      | OpenFOAM: The Open Source CFD
Toolbox   |
| \\      /  O p e r a t i o n  | Version:  2.3.0
|
|   \\ /    A n d          | Web:      www.OpenFOAM.org
|
|   \\/     M a n i p u l a t i o n  |
|
\*-----*-
-----*/
FoamFile
{
    version      2.0;
    format       ascii;
    class        dictionary;
    location     "system";
    object       controlDict;
}
// * * * * * * * * * * * * * * * * * * * * * * * * * * * * * * * * * * * * * * * * *
* * * * * * * * //
application    movingGridGasificationFoam;
startFrom      latestTime;

//startTime    0;

stopAt         endTime;

endTime        14400;

deltaT         0.05;

writeControl   timeStep;

writeInterval  2000;

purgeWrite     0;

writeFormat    ascii;

writePrecision 6;

writeCompression off;

timeFormat     general;
```



University of Moratuwa, Sri Lanka.
Electronic Theses & Dissertations
www.lib.mrt.ac.lk

```
timePrecision 6;

runTimeModifiable false;

//
*****
***** //
```



University of Moratuwa, Sri Lanka.
Electronic Theses & Dissertations
www.lib.mrt.ac.lk

Physical properties used for numerical solution: Physical properties dictionary

```

/*-----*- C++ -*-----
-----*\
| ===== |
| |
| \\      / F ield      | OpenFOAM: The Open Source CFD
Toolbox   |
| \\      / O peration  | Version: 2.3.0
|
| \\      / A nd        | Web:      www.OpenFOAM.org
|
|  \\/      M anipulation |
|
\*-----*-
-----*/

FoamFile
{
    version      2.0;
    format       ascii;
    class        dictionary;
    location     "constant";
    object       physicalProperties;
}
// * * * * * University of Moratuwa, Sri Lanka. * * * * *
* * * * * // Electronic Theses & Dissertations
* * * * * www.lib.mrt.ac.lk

// Solid properties

Solid_density      rhosolid [ 1 -3 0 0 0 0 0 ] 800;
Wood_density       Wooddensity [ 1 -3 0 0 0 0 0 ] 800;
Char_density       Chardensity [ 1 -3 0 0 0 0 0 ] 360;
Ash_density        Ashdensity [ 1 -3 0 0 0 0 0 ] 800;
Pyrolysis_temperature Tp [ 0 0 0 1 0 0 0 ] 473;
Activation_energy  E [ 1 2 -2 0 -1 0 0 ] 110e+3;
Frequency          f [ 0 0 -1 0 0 0 0 ] 1e+8;
Fiber_Saturation_Point Mfsp [ 0 0 0 0 0 0 0 ] 0.1;
Char_Fraction      CF [ 0 0 0 0 0 0 0 ] 0.178;
Volatile_Fraction VF [ 0 0 0 0 0 0 0 ] 0.8216;
Ash_Fraction       AF [ 0 0 0 0 0 0 0 ] 0.0004;
Initial_flame_time Tflame [ 0 0 0 0 0 0 0 ] 1200;
Specific_radiation_area Ar [ 0 -1 0 0 0 0 0 ] 1.5;
CO2fraction        CO2f [0 0 0 0 0 0 0] 0.54;
COfraction         COf [0 0 0 0 0 0 0] 0.4;
CH4fraction        CH4f [0 0 0 0 0 0 0] 0.0525;
H2fraction         H2f [0 0 0 0 0 0 0] 0.0075;
radiation_absorption_coefficient abs [0 -1 0 0 0 0 0] 0.375;
P1_model_Gamma    Gammar [0 1 0 0 0 0 0] 1/3;
steffans_constant steffb [1 0 -3 -4 0 0 0] 5.67e-8;

```

```

// Gas properties

Initial_Gas_density          rhogas [ 1 -3 0 0 0 0 0 ] 1.2;
Universal_gas_constant      R [ 1 2 -2 -1 -1 0 0 ] 8.314;
kH2O                        kH2O [ 0 0 0 -1 0 0 0 ] 0.003965;
kH2                          kH2 [ 0 0 0 -1 0 0 0 ] 0.0146;
kCH4                        kCH4 [ 0 0 0 -1 0 0 0 ] 0.009253;
kCO2                        kCO2 [ 0 0 0 -1 0 0 0 ] 0.008;
kCO                          kCO [ 0 0 0 -1 0 0 0 ] 0.012;
kO2                          kO2 [ 0 0 0 -1 0 0 0 ] 0.011;
kN2                          kN2 [ 0 0 0 -1 0 0 0 ] 0.0133;
MH2O                        MH2O [ 1 0 0 0 -1 0 0 ] 22.213;
MH2                          MH2 [ 1 0 0 0 -1 0 0 ] 3.74
MCH4                        MCH4 [ 1 0 0 0 -1 0 0 ] 20.622;
MCO                          MCO [ 1 0 0 0 -1 0 0 ] 28.5;
MCO2                        MCO2 [ 1 0 0 0 -1 0 0 ] 35;
MO2                          MO2 [ 1 0 0 0 -1 0 0 ] 30.43;
MN2                          MN2 [ 1 0 0 0 -1 0 0 ] 28.5;
sigmaH2O                    sigmaH2O [ 0 1 0 0 0 0 0 ] 3.176;
sigmaH2                      sigmaH2 [ 0 1 0 0 0 0 0 ] 3.269;
sigmaCH4                    sigmaCH4 [ 0 1 0 0 0 0 0 ] 3.7345;
sigmaCO                      sigmaCO [ 0 1 0 0 0 0 0 ] 3.7;
sigmaCO2                    sigmaCO2 [ 0 1 0 0 0 0 0 ] 3.826;
sigmaO2                      sigmaO2 [ 0 1 0 0 0 0 0 ] 3.589;
sigmaN2                      sigmaN2 [ 0 1 0 0 0 0 0 ] 3.755;
a                            a [ 0 0 0 0 0 0 0 ] 1760;
b                            b [ 0 0 0 0 0 0 0 ] 0;
c                            c [ 0 0 0 0 0 0 0 ] 0;
D                            D [ 0 1 0 0 0 0 0 ] 0.02;
Evapouration_Coefficient    Aw [ 0 0 -1 0 0 0 0 ] 5.56e+6;
Evaporation_Activation_energy Ew [ 1 2 -2 0 -1 0 0 ] 8.79e+4;
Ambient_Temperature        Ta [ 0 0 0 1 0 0 0 ] 300;
Relative_Humidity          RH [ 0 0 0 0 0 0 0 ] 0.7;
delta                      delta [ 0 0 0 0 0 0 0 ] 1e-25;
Aco2                      Aco2 [ 0 1 -1 -1 0 0 0 ] 3.42;
Ao2                        Ao2 [ 0 1 -1 -1 0 0 0 ] 0.652;
Hs                          Hs [ 1 -3 -1 1 0 0 0 ] 1;

//
*****
***** //

```



University of Moratuwa, Sri Lanka
 Electronic Theses & Dissertations
www.lib.mrt.ac.lk